DETECTING CEREBRAL DEGENERATION IN ALS USING A MULTICENTRE APPLICATION OF 3D TEXTURE ANALYSIS

By

Michael Chunn

A thesis submitted in partial fulfillment of the requirements for the degree of

Master of Science

Neuroscience

University of Alberta

Abstract

Amyotrophic lateral sclerosis (ALS) is a highly heterogeneous disease in terms of its clinical presentation, progression, and detected pathology in the body. It is a multi-system degenerative disorder, though a diagnosis is made based on the presence of both upper motor neuron (UMN) and lower motor neuron (LMN) degeneration. However, the disease rests on a spectrum of both motor and cognitive systems degeneration. ALS is fatal with a typical course of 2-5 years. The diagnostic process is long and complicated, often taking about one year from symptom onset. For these reasons, ALS needs a biomarker – an objective measure of disease presence and progression. This would simplify diagnosis and allow treatment and drug trials to be implemented earlier in the disease process. Studies have explored neuroimaging as a source of potential biomarkers. Techniques such as voxel-based morphometry (VBM) and diffusion tensor imaging (DTI) have been previously used to study cerebral degeneration but have yet to be refined as highly sensitive and specific diagnostic tools. A more novel tool called texture analysis (TA) has recently been applied to various diseases as a means to examine pathology *in vivo*. Furthermore, TA has been applied in two previous studies of ALS, finding high sensitivity and specificity in differentiating patients from controls. TA examines both grey matter and white matter in the brain simultaneously by quantifying the relationships between grey level intensities in neighbouring voxels of a 3D magnetic resonance image. It does so using T1-weighted images – often acquired as part of the diagnostic process. The present study aims to examine cerebral degeneration in ALS patients as detected by TA in a multicentre dataset, and how degeneration correlates with clinical signs of UMN degeneration. Furthermore, this study aims to test the reliability of TA both within and between sites of acquisition to further support the future implementation of TA as a clinical biomarker.

Preface

All research for this thesis was done under the supervision of Dr. Sanjay Kalra at the University of Alberta. Data derived from this thesis was published as:

- Preliminary Analyses: Chunn, M., Ishaque, A., Ta, D., Chenji, S., Mah, D., Seres, P., Yang, Y-H., Kalra, S. (2017). Detecting ALS Pathology Using 3D Whole-Brain Texture Analysis. Poster presented at Organization for Human Brain Mapping (OHBM), 2017. June 25-29, Vancouver, BC, Canada.

I, Michael Chunn, am responsible for constructing and performing the present analysis in addition to writing of this thesis and the associated poster published. Feedback was provided by my supervisor.

Acknowledgements

Firstly, I wish to thank my supervisor, Dr. Sanjay Kalra, for his patience and guidance throughout this research project. His valuable input, suggestions, and feedback helped to shape my work into something endlessly better than I could have done on my own. I am very grateful to have had the opportunity to work with him and to have had the chance to spend two years in an environment which allowed me so many other experiences for me to grow as a person. He pushed me in directions I wasn't always sure I could perform well in, but ultimately, I feel that I gained the confidence to tackle new and daunting situations.

I would also like to thank my supervisory committee for their guidance and input for my project. It was often helpful to have insight from a different perspective and this allowed me to shape my research to fill in gaps I hadn't considered. My lab members have also been a tremendous help in my work both in terms of their research collaboration and guidance, and in terms of the friendships that I made. They truly are a fantastic group of people and I'm lucky to have had a lab environment with such awesome people in it.

Additionally, I would like to thank those who provided funding for my research and to CALSNIC as a whole. CIHR and Brain Canada provided financial support for this research, and more specifically for my research I would like to thank Alberta Scholarships for the Queen Elizabeth II Graduate Scholarship and the Alberta Graduate Student Scholarship.

Finally, I would like to thank my family and friends, and my incredible girlfriend for all their endless support, patience, and encouragement throughout my research. It has been a lot of work getting here and I truly could not have done it without them. To all of you: Thank you for always listening when I needed someone to talk to. I am very lucky to have you in my life.

Table of Contents

List of Tables

List of Figures

Abbreviations

ACPC	Anterior commissure, posterior commissure
AD	Alzheimer's disease
ALS	Amyotrophic lateral sclerosis
ALSbi	ALS with behavioural impairment
ALSci	ALS with cognitive impairment
ALSFRS-R	ALS functional rating scale – revised
BPF	Brain parenchymal fraction
CALSNIC	Canadian ALS Neuroimaging Consortium
C9orf72	Chromosome 9 open reading frame 72
CNR	Contrast to noise ratio
CST	Corticospinal tract
DMN	Default mode network
DTI	Diffusion tensor imaging
EMG	Electromyography
FCD	Focal cortical dysplasia
FLAIR	Fluid attenuated inversion recovery
fMRI	Functional MRI
FSPGR	Fast spoiled gradient echo
FTD	Frontotemporal dementia
FTLD	Frontotemporal lobar degeneration
FUS	Fused in sarcoma
FVC	Forced vital capacity
GLCM	Grey level co-occurrence matrix
GM	Grey matter
H&E Stain	Hematoxylin-eosin stain

ICC	Intraclass correlation coefficient
LFB Stain	Luxol fast blue stain
LMN	Lower motor neuron
MMSE	Mini mental state examination
MRI	Magnetic resonance imaging
MPRAGE	Magnetization prepared rapid gradient echo
MS	Multiple sclerosis
PCG	Precentral gyrus
PD	Proton density
PET	Positron emission tomography
PMA	Progressive muscular atrophy
PLS	Primary lateral sclerosis
RLM	Run length matrix
SD	Symptom duration
SNR	Signal to noise ratio
SOD1	Superoxide dismutase 1
SPECT	Single-photon emission computed tomography
TA	Texture analysis
TE	Echo time
TARDBP	TAR DNA-binding protein
TR	Repetition time
UMN	Upper motor neuron
UPDRS	Unified Parkinson's disease rating scale
VBM	Voxel-based morphometry
WM	White matter

1. ALS

1.1. Disease Overview

Amyotrophic lateral sclerosis (ALS) is a motor neuron disease identifiable by degeneration of both upper motor neurons (UMN) and lower motor neurons (LMN). It is also known as Lou Gehrig's disease in the United States, and motor neurone disease in Europe. First described by Jean-Martin Charcot in 1887 [Turner, 2015], the disease is estimated to affect 2.16 in every 100 000 people based on European population studies [van Es, 2017]. Other population studies including that by Roberts et al. (2016) have indicated that the prevalence can be variable based on ancestral origin, though fewer studies have been carried out on non-European populations. Roberts (2016) explains that in the United States, white participants were at a significantly higher risk of ALS mortality than non-white populations. ALS is a highly heterogeneous disease, both in terms of its clinical presentation and its progression [Swinnen and Robberecht, 2014]. There is currently no cure for the disease, and it leads to death normally in 2-5 years from symptom onset. However, this is also quite variable with some patients progressing unusually slowly and some unusually quickly. Furthermore, the disease can present in a number of different ways. It is generally accepted now that ALS is a multisystem degenerative disorder that rests along a spectrum of diseases including several variants of ALS and frontotemporal dementia (FTD) [van Es, 2017; Strong, 2009]. Roughly 50% of all ALS patients develop some form of frontotemporal lobar degeneration (FTLD) which leads to cognitive and behavioural impairment [van Es, 2017]. In the most severe cases of cognitive decline, patients may go on to develop FTD as a comorbidity, in which case the diagnosis is termed ALS-FTD.

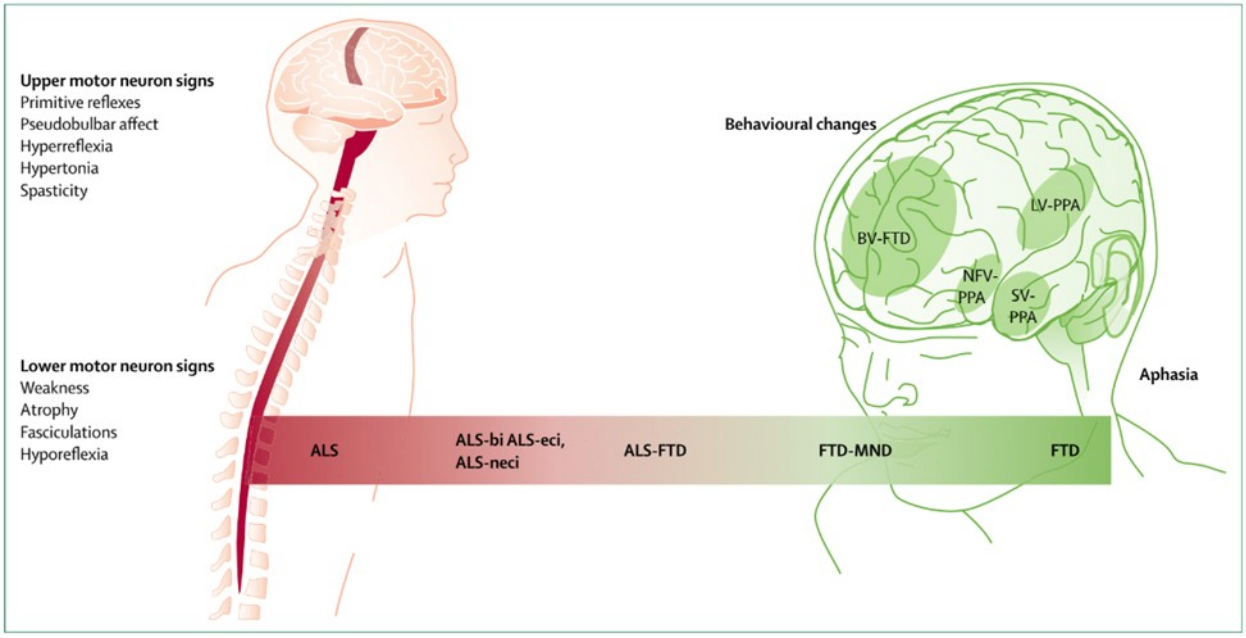

Figure 1. Representation of ALS disease spectrum and associated symptoms, taken from van Es et al. (2017).

Disease onset is typically after the age of 45 years, but in rare circumstances the disease may manifest in early adulthood as juvenile ALS which can affect people as young as 20 years [Turner, 2012]. The mean age of onset is slightly earlier for men than women (65 and 67 years old, respectively) [Langefeld, 2013; Turner, 2012]. Furthermore, the incidence and prevalence of the disease is higher in men, both of which show a ratio of 1.5:1 (men : women) [Wang, 2017]. However, Gordon et al. (2011) state in their study that this ratio is becoming more even in the recent years and suggest that women may now be more often exposed to environmental factors contributing to the manifestation of the disease. While it is unclear what exactly the cause of the disease is, there are a number of risk factors that have been identified as being possibly linked to ALS. One such environmental factor is the exposure to heavy metals such as lead and mercury. It was found that history of exposure to heavy metals was significantly elevated in ALS patients when compared with healthy controls in the same studies [Wang, 2017]. Another such risk factor is exposure to agricultural chemicals including pesticides and herbicides [Kamel, 2012]. Through

meta-analysis, it was found that people exposed to these types of chemicals had a 50% greater chance of developing ALS than those not exposed [Wang, 2017]. Studies such as that by Seals et al. (2016) have even suggested that head trauma at least 5 years prior to ALS onset can be a risk factor in the manifestation of the disease. They go on to suggest that this might put certain professions at greater risk of developing ALS, such as professional athletes and military veterans [Seals et al. 2016]. A number of studies have also identified cigarette smoking as a risk factor in ALS [Fang et al. 2009; Okamoto et al. 2009]. However, the meta-analysis performed by Wang et al. (2017) has noted that while there may be some mild risk associated with smoking, it is likely as low as increasing chances to 1.3 times the normal risk. It has been suggested that some socioeconomic factors can be influential in the development of ALS. Roberts et al. (2016) state that even once adjusted for race/ethnicity, higher level of attained education such as university and post-graduate training were positively associated with increased risk of developing ALS. In contrast, some studies have identified potential mild protective factors against ALS such as consumption of coffee and vitamin E [Beghi et al. 2011; Freedman et al. 2013].

The diagnostic process is heavily reliant on neurological examination in clinic and is complicated by the heterogeneity in presentation of symptoms. ALS diagnosis is dependent on the clinical presentation of both UMN and LMN signs in at least one of four regions of the body – bulbar, cervical, thoracic, and lumbosacral – and until both are detected, a definite diagnosis cannot be made. For this reason, the process can often be delayed by roughly one year from symptom onset. A diagnosis of ALS typically made dependent on the El Escorial criteria for ALS, though some other criteria exist including the Awaji criteria which includes a greater emphasis on electrodiagnostic tools. Diagnosis based on the El Escorial criteria splits patients into several different designations based on how certain their diagnosis is. Suspected ALS is

defined as the presence of LMN signs in two or more regions. Possible ALS is given if the patient presents with LMN signs and UMN signs in only one region of the body, or if UMN signs are present in two regions. Probable ALS is defined as the presence of LMN and UMN signs in at least two regions each. Lastly, a patient is diagnosed with definite ALS if LMN and UMN signs manifest in the bulbar region as well as at least two other regions of the body. However, these diagnoses can only be made in the absence of other clinical or electrodiagnostic evidence that the signs and symptoms are not caused by another pathological process. Disease mimics can be one of the major confounding and complicating factors of the diagnostic process. Some common disease mimics of ALS are primary lateral sclerosis (PLS), a motor neuron disease only affecting UMN of the body, and progressive muscular atrophy (PMA), which only affects the LMN. Other diagnoses which can present with similar symptoms include spinocerebellar ataxia, and various neuropathies leading to muscle weakness and ALS-like abnormalities.

As mentioned, one of the major complicating factors in ALS diagnosis is the variable presentation of pathological signs. Signs of LMN degeneration include weakness and atrophy of muscles, fasciculations, cramps, and loss of reflexes due to muscle loss. Muscle loss can also occur in the muscles of respiration – often the cause of death in ALS patients. UMN pathology presents in the form of spasticity, brisk reflexes, clonus, and pathological reflexes such as Babinski's sign. Furthermore, there are a number of bulbar-related symptoms such as slurred speech, and difficulty swallowing. Depending on the first symptoms that present, ALS is divided into two onset types. Of the roughly 70% of patients present with classic ALS, 33% suffer from bulbar onset [van Es, 2017]. This characterised by difficulty with speech and swallowing. In contrast, limb onset (66%) is characterised by the weakness and loss of dexterity

in the limbs where patients often notice awkwardness in walking or inability to lift objects [van Es, 2017]. Additionally, a less common (3%) variant is termed respiratory onset ALS, which begins with a degeneration of the muscles of respiration – a symptom that typically develops late in the disease process – and is often associated with a poorer prognosis [van Es, 2017].

1.2. Genetic Contributions

ALS patients are split into 2 categories: familial (10%) and sporadic (90%). There have been a number of genes that have been identified as being linked to ALS. Among the familial ALS patients, roughly 60-80% of patients have an identifiable genetic mutation contributing to their development of the disease. The first major genetic factor identified was the SOD1 gene and is identified as the predominant cause of disease in 20% of these patients with an identifiable genetic component. Other genetic variations that have been identified since include the C9orf72 which is now known to be the most common genetic factor (40%), TARDBP (1-5%), and FUS genes (1-5%) [van Es, 2017; Al-Chalabi, 2012]. Genetic involvement in ALS is also not entirely clear. The most common genetic cause of ALS is the C9orf72 mutation which is present in roughly 40% of familial cases and 10% of patients labelled as sporadic [van Es, 2017; Swinnen, 2014]. Furthermore, the immediate family members of these sporadic ALS patients are at an increased risk of developing ALS themselves [van Es, 2017]. Genetic studies are also further complicated by phenotypic heterogeneity in ALS patients [Swinnen and Robberecht, 2014]. Involvement of different genes is spread across the ALS disease spectrum, and while the presence of one mutation can be predictive of presenting phenotype it does not guarantee the manifestation of it. There has recently been a greater acknowledgement of the overlap in disease process and pathology for ALS and FTLD and how they might be linked in their underlying genetic contributions [Al-Chalabi, 2012]. Additionally, as previously stated, there are a number

of environmental risk factors that have been identified as potential contributors to the manifestation of motor neuron degeneration. There is often an interplay of both genetic and environmental factors in the development of any disorder or disease. While someone may carry a particular mutation, they may require the presence of any risk factor or stressor for the disease to develop. Conversely, a person may live their entire life exposed to one of the previously mentioned risk factors and not develop the disease as there was no susceptibility present for them. There is a significant interplay between the genetic component and the environmental component of ALS that is not entirely understood. This is another complicating factor in the diagnostic process, as it is difficult to determine with absolute certainty the cause of a patient's symptoms based solely on the genetic and environmental factors that they have present in their life.

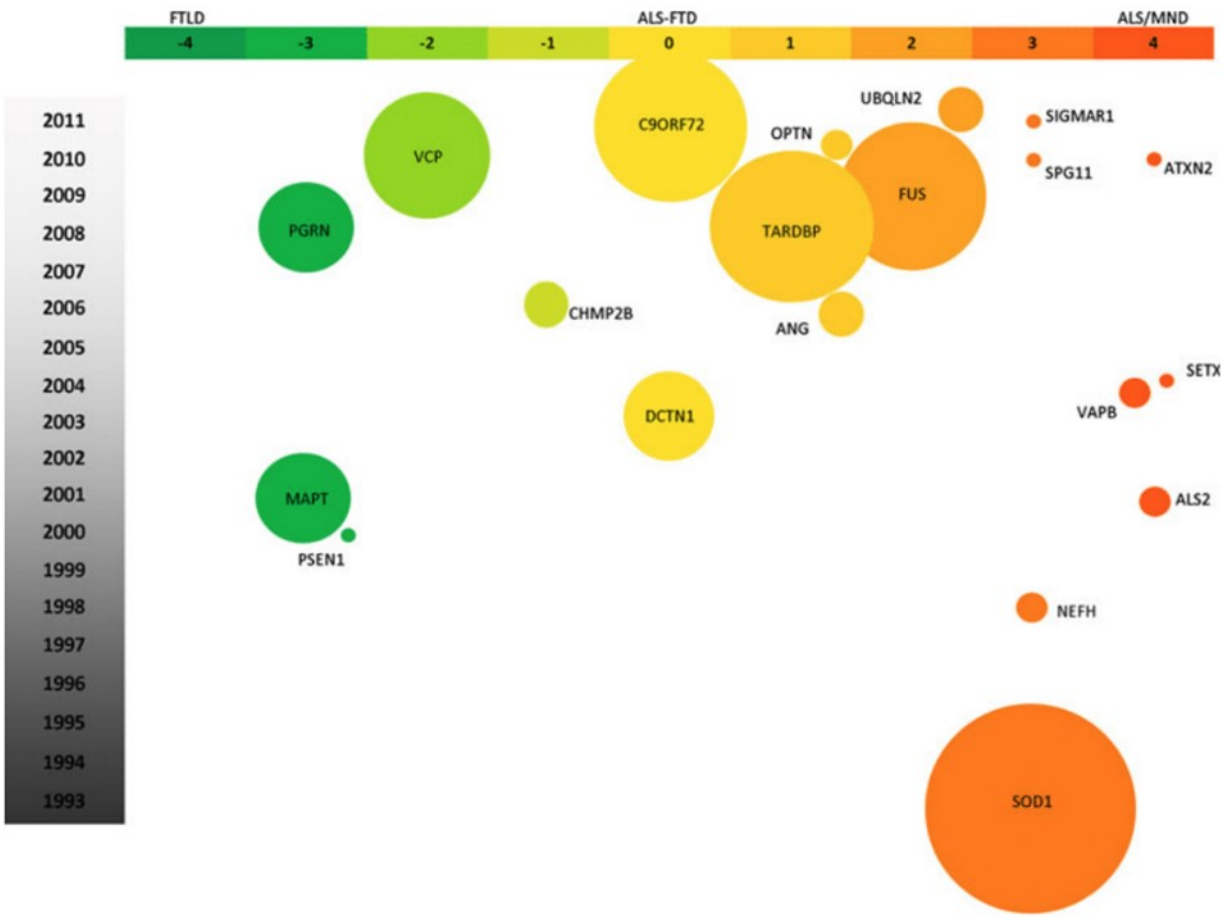

Figure 2. Representation of variable genetic involvement along the ALS disease spectrum, taken from Al-Chalabi et al. (2012).

1.3. Pathogenesis

Little is known for certain about the pathogenesis of ALS. However, ongoing research points toward several possible mechanisms leading to cerebral degeneration and progression of the disease. One of these possible mechanisms is glutamate excitotoxicity [Introna, 2018; Kumar, 2016]. This process works by a cascading mechanism in which overstimulated cells release large amounts of glutamate. Pathologically high levels of glutamate or other excitatory molecules which bind to NMDA glutamate receptors can alter intra-cellular levels of Ca^{2+} ions, leading to degenerative processes in the cells [Jaiswal, 2009]. Furthermore, upon death of any affected cell, its contents may be released into the extracellular space, triggering an excessive

release from neighbouring cells due to receptors on the extracellular membrane [Manev, 1990]. This process can lead to spread of cell death via adjacent cells.

In addition to the excitotoxic hypothesis, it has been suggested that the involvement of mutant Superoxide Dismutase 1 (SOD1) in ALS patients could be harmful in other ways than just the lack of functional enzyme. SOD1 is typically involved in apoptotic processes in its removal of harmful superoxide products from cells [Sea, 2015]. It has been suggested that the SOD1 mutant form found in ALS patients could be toxic to neuronal cells. Furukawa and O'Halloran (2005) state that mutant SOD1 is unstable and easily reduced, leading to both an inability to perform its enzymatic function and an aggregation of these mutant proteins in the cytoplasm of neuronal cells. These cytoplasmic aggregations have been detected on several occasions in familial ALS patients [Furukawa, 2005]. It has also been proposed that a possible mechanism of ALS pathogenesis is via SOD1 mutated glial cells [Julien, 2007]. Julien's paper goes on to explain that while SOD1 mutation in neuronal cells is more likely involved in disease onset, the affected and adjacent microglial and astrocytic cells are involved in the progression and exacerbation of the disease process. This might be due in part to reactive oxygen species present in the mutant glial cells, but also due to ineffective clearance of glutamate from the extracellular space by these astrocytes [Julien, 2007].

One mechanism more recently associated with ALS is the involvement of TDP-43 protein aggregation. Cytoplasmic TDP-43 inclusions have also been implicated as a point of overlap in both ALS and FTD pathology, indicating a link in the pathology for these diseases along the spectrum of disorders [Rothstein, 2009]. Furthermore, mutation of the TAR DNA-binding protein (TARDBP) gene and TDP-43 protein inclusions have been identified in both sporadic and familial cases of ALS [Rothstein, 2009]. TDP-43 is a protein most often found in

cell nuclei which is involved in RNA transcription and regulation of gene splicing mechanics [Mackenzie, 2010]. Mackenzie explains that the typical presentation of TDP-43 abnormalities in ALS patients is the presence of cytoplasmic aggregates in the motor cortex and associated fiber tracts leading into the spinal cord, and as one might expect in cases of FTLD, these inclusions are also found in the frontotemporal cortical regions as well as in some cases the dentate gyrus. Apart from inclusions, animal cell models have shown that in the presence of mutant TDP-43, muscle strength is reduced with observed motor disturbances [Kraemer, 2010].

Similar to TARDBP, recent research has gone into the Fused in Sarcoma (FUS) gene as a source of the pathological process in ALS. Mackenzie (2010) states that normally the FUS gene is involved in several cellular processes such as "cell proliferation, DNA repair, transcription regulation, and RNA and microRNA processing." In cases where the gene is mutated, much like SOD1 and TARDBP, intracellular inclusions are found [Mackenzie, 2010]. Furthermore, Vance et al. (2009) state that FUS pathology appears to be widespread, with FUS-mutated patients experiencing loss of neuronal cells in the spinal cord, brainstem, and motor cortex. Furthermore, this pathology included a spread of inclusions to glial cells, and in some cases there has been evidence of mild demyelination [Vance, 2009]. These findings were in the absence of both TDP-43 protein aggregation and cognitive changes, indicating an independent pathological process.

The most common genetic cause of ALS is the chromosome 9 open reading frame 72 (C9orf72) mutation which is a pathogenic hexanucleotide expansion [Maurel, 2018]. Normal function of the healthy protein is not well understood, but the mutation manifests as neuronal inclusions which may in turn be toxic to the cells [Maurel, 2018]. As is the case with both SOD1 and FUS, C9orf72 inclusions are often ubiquitin-positive, and the C9orf72 inclusions are found in both brain and skeletal muscle tissue [Maurel, 2018]. Ubiquitination of proteins is a form of

post-translational modification which is known to have a role in degradation, but also protein binding and interaction [Komander, 2009; Natarajan and Takeda, 2017]. It has been suggested that a deregulation of the ubiquitin system in ALS is responsible for progressive degeneration of motor neurons, and further that the hexanucleotide expansion in the C9orf72 mutation contributes to this impairment of the ubiquitin system [Maurel, 2018]. C9orf72 inclusions have also been noted to test positive in the cerebellum, hippocampus, and frontotemporal regions for p62, a protein involved in autophagy [Al-Sarraj, 2011; Maurel, 2018].

1.4. Pathology

In terms of gross anatomical changes, the brains of ALS patients appear to be largely unaffected. Few studies in ALS have detected gross atrophic changes in the brain, though some atrophic changes have been reported in the precentral gyrus as detected by post mortem and imaging studies [Saberi, 2015; Rajagopalan, 2014; Devine, 2015; Bede, 2013]. Atrophy appears to be the most substantial in patients who experience comorbid dementia or cognitive changes due to FTLD, in which case atrophic changes are seen in the frontal and temporal lobes of the brain [Saberi, 2015; Rajagopalan, 2014; Kim, 2017; Masuda, 2016; Lillo, 2012; Chang, 2005]. Furthermore, atrophy is known to occur in the spinal cords of ALS patients [Branco, 2014; Saberi, 2015]. Apart from gross atrophy, studies have noted neuronal loss and degeneration in the precentral gyri, as well as the CST [Saberi, 2015; Eisen, 2001]. However, degenerative processes in the WM of ALS patients seem to be largely microscopic changes rather than gross atrophic changes. Saberi (2015), suggests that ALS, on a microscopic level, leads to both neuronal and axonal loss. In contrast, reactive astrogliosis – an abnormal increase in astrocytes – is known to occur in areas of neuronal loss [Saberi, 2015]. While ALS is not a demyelinating disorder, both studies of diffusion imaging and tissue samples have noted pathological changes

in CST myelin of ALS patients [Sugiyama, 2013; Chapman, 2014]. Studies including that by Stephens et al. (2006) have also noted that there is significant neuronal loss in the ventral horn of the spinal cord when compared with healthy controls. Neuronal loss in the spinal cord is inclusive of myelinated axons, and this can be visualised in tissue samples using Luxol fast blue stains [Saberi, 2015]. Furthermore, they noted that there was a loss of interneurons in the dorsomedial quadrant of the spinal cord. Other changes on the cellular level include a loss of cortical Betz cells in the precentral gyrus, as well as a degeneration of pyramidal cells in medullary regions [Eisen, 2001; Hammer, 1979]. Betz cell loss in the cortex is best seen using H&E stains [Saberi, 2015]. Bunina bodies, which are small intracellular inclusions, have also been observed in motor neurons of the brain and spinal cord, though their significance is not well understood [Saberi, 2015]. Intracellular, ubiquitin-positive inclusions are common in ALS with different genetic variants of the disease contributing to this [Al-Chalabi, 2012]. Pathological protein aggregations are known to be associated with, SOD1, TARDBP, FUS, and C9orf72 mutations and can occur throughout the brain [Furukawa, 2005; Rothstein, 2009; Mackenzie, 2010; Maurel, 2018]. Many of their effects are discussed in Section 1.3. Additionally, in some cases ALS patients may present with tau protein pathology in the amygdala and entorhinal cortex, though this is more common in patients who develop cognitive impairment [Al-Chalabi, 2012; Strong, 2006]. Saberi et al. (2015) notes that other forms of pathology seen in ALS are cellular changes such as shrinking of neurons, vacuolisation, and spongiosis. However, vacuolisation – an increase in large, empty spaces in areas adjacent to neurons that are degenerating – is rarely seen apart from in rapidly progressing patients [Tandan and Bradley, 1985; Saberi, 2015].

The spatial distribution of pathological changes in the brain is variable, though the most widely recognised degeneration occurs in the motor cortex and the descending motor tracts starting at the CST. In cases of cognitive decline, studies have demonstrated degeneration of the prefrontal cortex and the temporal lobe [Lillo, 2012; Chang, 2005]. However, detected abnormalities in imaging studies can be widespread and can occur in structures such as the cerebellum, the thalamus, the basal ganglia, and other deep brain structures [Kim, 2016; de Albuquerque, 2016; Masuda, 2016]. Brettschneider et al. (2012) state that apart from the motor regions, some of the most common areas of pathology in both ALS and FTLD are the amygdala, the hippocampus, the middle frontal gyrus, and the middle and superior temporal gyri. Furthermore, extra-motor and subcortical regions seem less affected by neuronal loss compared to the motor cortex and spinal cord [Brettschneider, 2012]. Microglial activation, which is associated with neuroinflammation, is also known to occur in the motor and extra-motor regions of the brain [Brettschneider, 2012]. Additionally, Brettschneider et al. (2012) linked microglial activation and TDP-43 pathology in the extra-motor regions to reduced performance on neuropsychometric testing. Microglia in the brain act against neuronal distress by releasing proinflammatory molecules including reactive oxygen species [Saberi, 2015]. Neuroinflammation appears to have both helpful and harmful effects in the brain and can be responsible for some degeneration [Saberi, 2015]. Brettschneider et al. (2013) additionally proposed a model for the progression of TDP-43 pathology which aims to provide a basis of understanding for the spread of this pathology in ALS patients. It begins in the motor cortex and brainstem and spreads outward to involve extra-motor regions including the hippocampus.

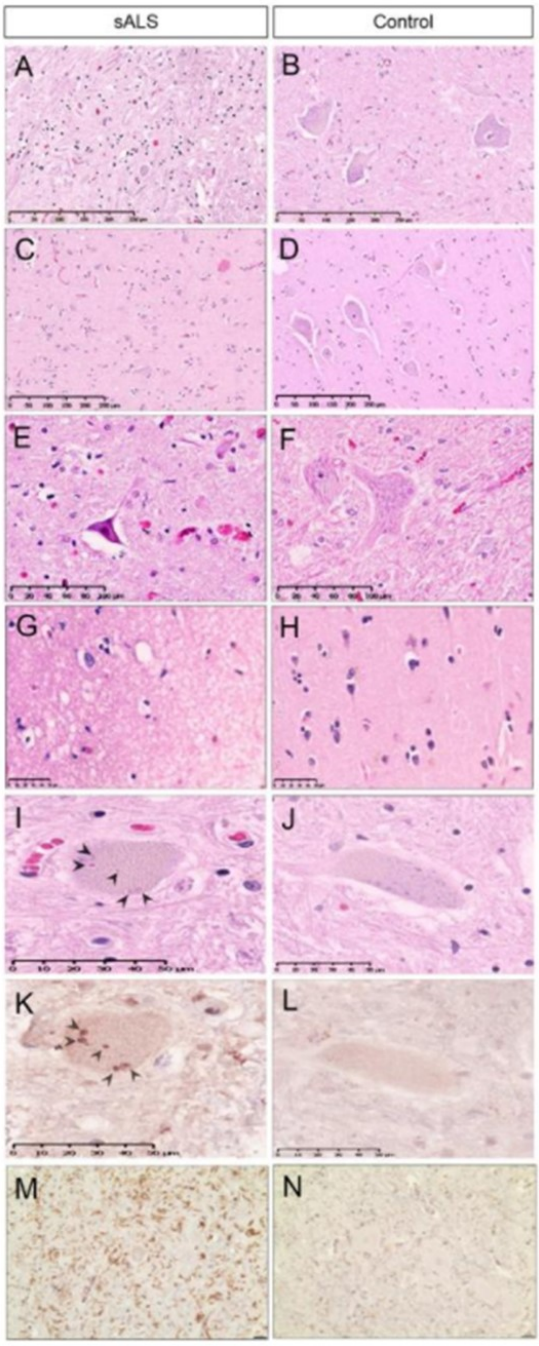

Figure 3. Typical neuropathology seen in sporadic ALS patients compared to healthy controls, taken from Saberi et al. (2015). Panels *A* – *J* are H&E stains. *A* and *C* demonstrate loss of motor neurons and astrogliosis in the spinal cord and motor cortex, respectively. *E* shows shrinking and contraction of motor neurons, *G* shows vacuolisation and spongiosis, and *I* demonstrates the presence of Bunina bodies. *K* and *M* present staining for cystatin c in Bunina bodies and microglial activation, respectively. Panels *B*, *D*, *F*, *H*, *J*, *L*, and *N* all show the absence of these pathologies in healthy controls.

1.5. Clinical Signs of ALS

As mentioned in the Disease Overview section, there are a number of signs and symptoms that are characteristic of UMN and LMN degeneration. One of the most obvious signs of LMN degeneration in patients is a general atrophy of muscle tissue. This can lead to cramps, or weakness and a loss of dexterity in movement. Many patients will notice an inability to lift

objects or themselves after falls, or they may notice clumsiness in walking. Patients may also notice a foot drop in walking which can sometimes lead to tripping. Additionally, this muscle weakness can affect the muscles of speech, leading to slurred or nasal speech known as dysarthria. Eventually dysarthria can progress to a point of inability to produce speech, in which patients require the use of adaptive forms of communication. Furthermore, patients may experience difficulty in or an inability to swallow, known as dysphagia. As the disease progresses, the muscles of respiration begin to degenerate. As mentioned, respiratory failure is often the cause of death in ALS patients. Another sign of LMN degeneration is the appearance of fasciculations in the muscles – small, involuntary, and repetitive twitches which are visible at the surface of the skin. These are often visible in any of the limbs, and occasionally also in the tongue. Physicians may also notice a decrease in reflex response if muscles that support the movement begin to degenerate.

In contrast, a major sign of UMN degeneration is hyperreflexia – an increased reflex response. UMN activity is typically a regulatory mechanism for voluntary and reflexive movements, and with a degeneration of these neurons the movements become more exaggerated or repetitive. One such repetitive response is clonus. This is identifiable if upon a rapid flexion of the wrist or the ankle, the hand or foot jerks back and forth a number of times. Another common sign of UMN degeneration in ALS is Babinski's Sign. In this abnormal response to stimulation of the sole of the foot, the normal downward flexion of the big toe is replaced by upward extension. A similar pathological reflex also seen in the presence of UMN degeneration is the Hoffmann's Reflex. This is tested by holding underneath the middle finger, pressing down on the nail, and allowing it to flick up naturally upon release. If there is a flexion of the terminal joint of the thumb on the same hand, this indicates the presence of UMN pathology. Apart from specific

abnormal reflexes, other reflexes tested may become pathologically brisk relative to a normal response to the same type of stimulation. Unfortunately, reflex measurement can be somewhat subjective given that there is variation in the strength of reflex responses between individuals. For instance, a healthy subject might have a relatively brisk reflex with no pathology present. In addition to hyperreflexia, patients with UMN degeneration may experience spasticity in their muscles, which is a constantly increased muscle tone. This can occur in the limbs, but also in the muscles of speech and swallowing, further contributing to dysarthria and dysphagia experienced due to LMN involvement. Patients who first experience symptoms such as these are characterised as limb-onset ALS.

In addition to these LMN and UMN signs, ALS can spread into extra-motor areas in cases of FTLD. ALS with FTLD is typically separated into two subcategories: ALS with behavioural impairment (ALSbi), and ALS with cognitive impairment (ALSci). Cognitive impairment-related degeneration in ALS typically affects areas such as the prefrontal cortex which can contribute to impaired performance on executive function tasks. Executive function involves cognitive processes such as task switching, working memory, attention and inhibitory control, and behavioural planning. Specific tasks showing deficits in ALS often include semantic and verbal fluency, alternation tasks, and social cognition. Conversely, behavioural impairment in ALS is characterised by disinhibition leading to socially inappropriate behaviour, apathy, and a general loss of empathy or sympathy [Rascovsky et al. 2011]. These symptoms can typically be assessed using behavioural observer checklists as well several social and affect-related questionnaires.

In addition to these motor and cognitive manifestations of the disease, some patients experience bulbar dysfunction. Patients who notice this type of symptom first are described as

having bulbar-onset ALS. This bulbar involvement in ALS typically manifests as a degeneration of the muscles of speech and swallowing. Furthermore, this can include change in levels of salivation or a general difficulty with clearing it. This is of particular importance in MRI related studies given that for patients who experience a large amount of salivation. Combined with difficulty swallowing, it can be difficult to lay still for an extended period of time without risking choking, or at the very least some significant movement in order to clear it. For that reason, there is an unintentional bias toward recruiting patients with less bulbar involvement in MRI studies. A slightly rarer manifestation of bulbar degeneration in ALS is in the instance of corticobulbar degeneration. In these cases, patients may experience symptoms of pseudo-bulbar affect. These symptoms include inappropriate and uncontrollable laughter or crying [Demler, 2017].

1.6. Treatment and Management

Currently, there is no cure for ALS. Furthermore, there is only one drug currently prescribed to ALS patients. Riluzole acts by blocking excitatory action of glutamate with the goal of minimizing excitotoxic activity [Martin, 1993]. Glutamate is one of the major excitatory neurotransmitters of the brain, and excess release can lead to excitotoxic activity leading to cell death [Jaiswal, 2009, Manev, 1990]. Riluzole has been shown to have modest success at slowing disease progression, though these results have been inconsistent [Keating, 2016]. Keating (2016) details a number of studies of riluzole which show varied success, though results show the drug slowing progression by 4-19 months on average. In addition, a newer drug called edaravone has been recently approved by the Food and Drug Administration [Introna, 2018]. A number of other clinical drug trials have screened possible strategies for managing the disease, but few have had any greater success [Kumar, 2016]. Thus, much of the disease management for ALS is a process

of maintaining patient quality of life in the degenerative process. Due to weakness in the respiratory muscles, many patients require ventilators such as BIPAP machines.

1.7. Need for Biomarkers

ALS is in desperate need of a biomarker – some form of measure which can indicate a departure from normal physiological process. An ideal biomarker candidate is something that can objectively measure presence and progression of pathology with little experimental error. They can be anything from blood, urine, or CSF content to neuroimaging-based sources. The best method currently used to track disease progression is the ALSFRS-R scale, which typically shows a decreasing trend of 1 point per month. However, the ALSFRS-R is primarily a measure of dysfunction related to LMN involvement and can also be somewhat subjective. Moreover, the ALSFRS-R is not a diagnostic test and still requires clinical examination to determine ALS to be the cause of symptoms. Thus, it does not meet the requirements of being a biomarker. There are several current biomarker candidates for ALS, though none of these have been – as of yet – fully validated. One of the most promising candidates is CSF neurofilament content. Neurofilaments are an important factor in axonal integrity, and their dysfunction is thought to be involved in the degeneration of motor neurons [Turner, 2009]. Elevated CSF neurofilament content is seen in ALS patients when compared to healthy controls and even disease mimics [Turner, 2009]. Additionally, while some studies have examined change in neurofilament levels over time, more research must be done to determine if they can reliably be used as a measure of disease progression [Vu and Bowser, 2017]. Though this is a promising biomarker with relatively high sensitivity and specificity for diagnosis, taking CSF samples is rather invasive and there may be a risk of infection. Perhaps less invasively, neurofilament levels can also be measured through blood samples, which can also be of use for the prognosis of disease progression rate and

survival [Vu and Bowser, 2017]. Blood and CSF can also be used to measure levels of inflammatory factors and MicroRNAs, and while these can be linked to disease presence, they do not yet offer any substantial improvement of sensitivity and specificity [Turner, 2009; Vu and Bowser, 2017]. Urine content may also be a novel and non-invasive source of biomarkers [Vu and Bowser, 2017]. One of the more recent and promising candidates is neurotrophin receptor p75 (p75NTR) which is known as a regulator of cell survival [Shepheard, 2014]. Shepheard et al. (2014) suggest that p75NTR appears in increased levels in the urine of ALS patients and also correlates with disease progression and severity measured by ALSFRS-R. However, p75NTR has not yet been studied in great detail and requires further testing. Neuroimaging has been seen recently as a new and exciting source of biomarkers for ALS. Techniques such as VBM and DTI have been used to examine structural degeneration in the brain [Prudlo, 2012; Masuda, 2016; Rajagopalan, 2014; Bede, 2013]. Despite high costs of operation and limited availability in some centres, MRI is minimally invasive and relatively easy to implement in clinic. This makes it an appealing source of biomarkers. Electrodiagnostic tests such as electromyography (EMG) have also been recognised as a means to study LMN burden at the level of the muscle fibre [de Carvalho and Swash, 2011]. EMG along with another technique called electrical impedence myometry have been suggested to be potential measures of survival and disease progression, respectively, though more research must be done to validate them as biomarkers of the disease [de Carvalho and Swash, 2011]. Objective measures allow for diagnoses to be made more quickly and with greater certainty. Additionally, biomarkers allow for more effective monitoring of disease progression which is crucial in the development of new treatment strategies – namely in drug trials. In the case of ALS, drug trials can only include patients once they have been diagnosed, something that often only occurs a year or more after symptom onset. This means that

the pathology has already progressed significantly. If a truly effective biomarker is found for ALS it would allow an earlier diagnosis, and thus an earlier initiation of drug trials with the potential of catching the disease at a point of vulnerability to treatment. Furthermore, biomarkers enable the implementation of drug trials with less participants involved. This is based on the consideration that a biomarker would reduce experimental error, which in turn reduces the numbers required for meaningful statistical results.

2. Magnetic Resonance Imaging in ALS

2.1. Structural Imaging

MRI imaging works on the premise of exciting the protons in the imaged tissues using a radio frequency pulse in a strong magnetic field, and then examining the varying rates at which these molecules relax back to their initial state [Jackson, 1997]. These different rates of relaxation are what allows a differentiation between tissue types in the body based on their respective compositions. In structural MRI different relaxation properties of individual tissue types contribute to the image contrast acquired [Jackson, 1997]. T1 relaxation refers to the reorientation of the protons resulting in a recovery of longitudinal magnetisation [Preston, 2006]. In contrast, T2 relaxation is the desynchronization of proton spins resulting in the decay of transverse magnetisation [Preston, 2006]. Image acquisition parameters can be manipulated in order to emphasize either of these two types of relaxation in the image. Repetition time (TR) and echo time (TE) are the two main factors manipulated by technologists in order to obtain different types of structural images [Jackson, 1997]. For brain imaging, there are several forms of standard structural imaging techniques which are effective at analysing anatomy and pathology. T1-weighted images are acquired using a short TR and TE and are excellent for imaging of anatomy as they are the most representative of the way tissues appear macroscopically in the brain [Preston, 2006, Abdulla, 2017]. T2-weighted images are acquired using a long TR and TE, and they are useful for examining pathology and lesions associated with increased water content such as hemorrhaging [Preston, 2006; Abdulla, 2017]. An even longer TR and TE produces a fluid attenuated inversion recovery (FLAIR) image in which pathological abnormalities appear bright while CSF appears darker [Preston, 2006]. Proton density (PD) weighted images use a mixture of long TR and short TE in order to obtain a clear tissue contrast with defined, visible lesions,

though they have been more or less replaced by FLAIR [Jones, 2016; Abdulla, 2017]. Structural imaging can be quite useful in the diagnostic process for different types of pathology. For instance, PD weighted, T2-weighted, and associated sequences are very effective at detecting pathological lesions in multiple sclerosis (MS) patients which appear as hyperintense regions in the image [Maggi, 2018; Rashid, 2008].

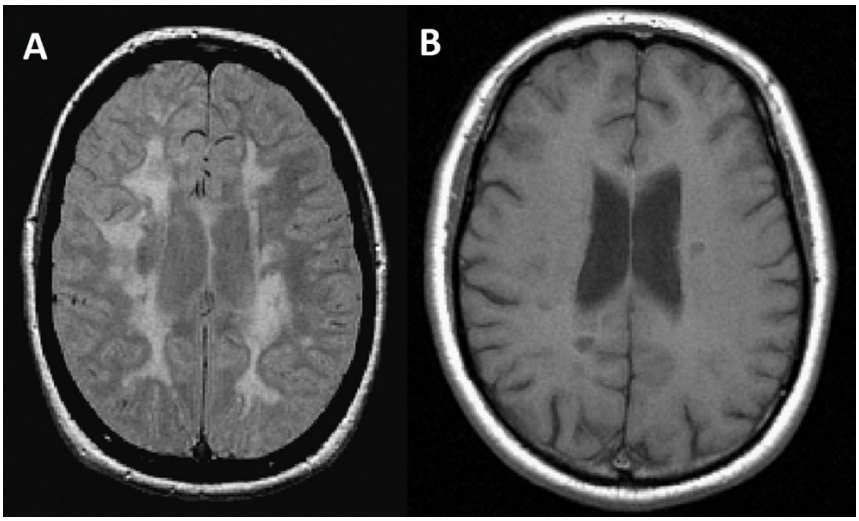

Figure 4. MS lesions as detected by neuroimaging – images extracted from Rashid et al. (2008). A) Lesions appear as hyperintense regions in PD weighted images. B) Lesions appear as hypointensities in T1 image.

T1-weighted images are useful for examining the relatively overt atrophic degeneration seen in Alzheimer's disease (AD) patients [Jack Jr., 2008; Dustin, 2016], but it is also possible to see MS lesions on these images presenting as hypointensities in this case [Rashid, 2008].

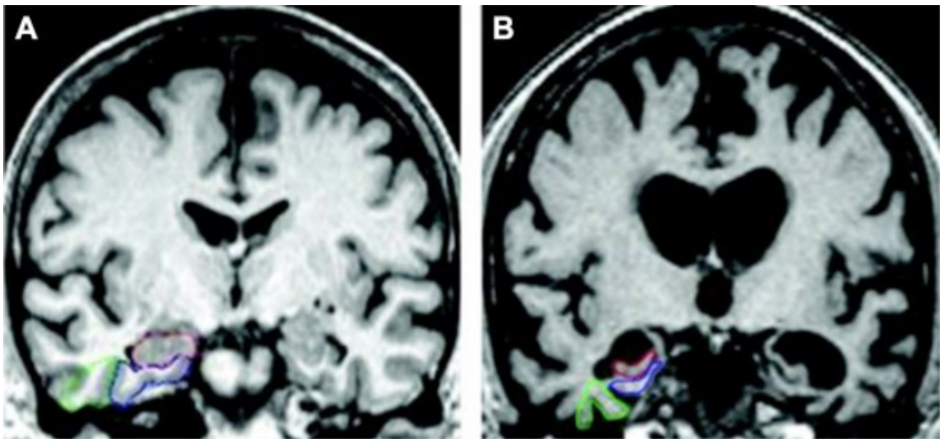

Figure 5. Alzheimer's disease pathology compared with healthy control in T1-weighted imaging – taken from Dustin et al. (2016). Coloured regions trace the different hippocampal subfields and are meant to demonstrate atrophy of these regions. A) T1 scan of healthy control with ROIs for medial temporal lobe volumetric measurements. B) T1 scan of AD patient demonstrating significant medial temporal lobe – and global – atrophy.

In contrast to these neurological disorders, ALS patients inconsistently show any differences from healthy controls on conventional structural imaging. Some studies have demonstrated signal intensity changes in the CST on T1 and T2 images [Hecht, 2001; Chio, 2014; Waragai, 1997]. More specifically, Keller et al. (2011) state that there have been instances of hyperintensities in the posterior limb of the internal capsule detected in T2 and FLAIR images. In some cases, ALS patients may also present with hypointense rims around the precentral gyrus using T2 images [Chio, 2014; Keller, 2010]. Furthermore, in the examination of T1 and T2 images, it is not uncommon that no signal intensity changes are present at all. Hecht et al. (2001) note that T1 signal intensity changes were present in only 3 of 31 total ALS patients, compared to detected hypointensities in 20 healthy controls. They state that FLAIR images were more consistently able to detect signal intensity changes in patients, though these changes are also present in a number of healthy controls [Hecht, 2001]. The presence of signal intensity changes in healthy controls greatly reduces specificity and is problematic for the employment of

conventional structural imaging sequences as a means of diagnosis [Kalra and Arnold, 2003; Hecht, 2001; Abe, 1993]. Sensitivity and specificity in structural imaging studies are variable, but they are most often moderate to low in value [Grosskreutz, 2008; Kalra and Arnold, 2003; Kassubek, 2012]. Gupta, et al. (2014) report an overall sensitivity and specificity for CST hyperintensity of 48% and 76%, respectively, using conventional sequences. Depending on the portion of the CST in question, specificity values ranged from 32-92%. While signal intensity changes may be indicative of ALS pathology, they cannot be used as a firm or reliable diagnostic tool [Chio, 2014; Keller, 2010]. Physician examination of structural images may also introduce a certain level of subjectivity. For these reasons, structural MRI sequences are employed in the diagnostic process only as a means to rule out other causes of pathology [Chio, 2014; Kassubek, 2012].

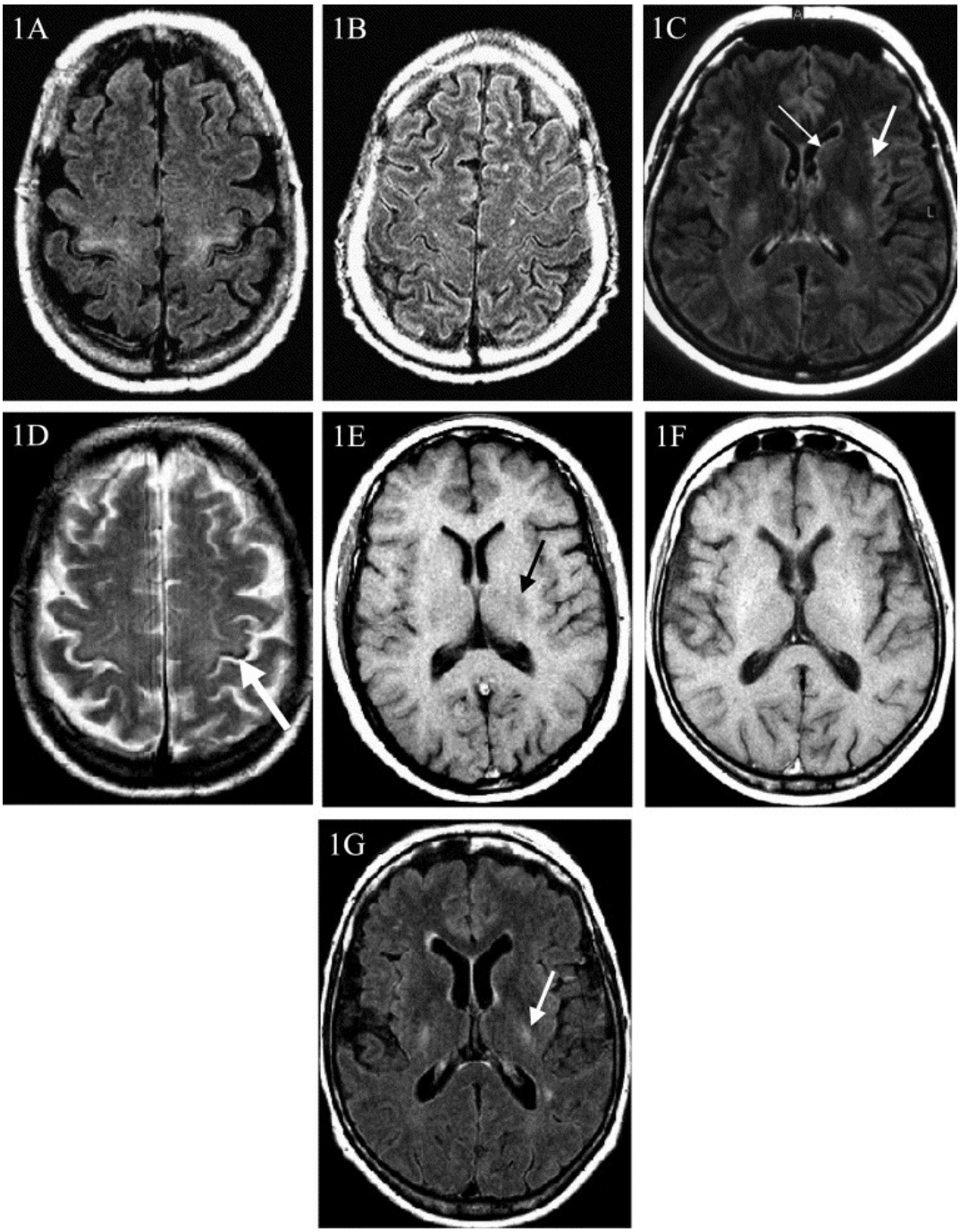

Figure 6. ALS patients compared with healthy controls in various conventional MRI sequences, taken from Hecht et al. (2001). Panels *1A* and *1C* demonstrate hyperintensities in FLAIR images of ALS patients in the precentral gyrus and the insula, respectively. *1D* shows T2 hypointensity at the precentral gyrus. *1F* and *1G* are images of the same patient showing T1 isointensity and FLAIR hyperintensity of the internal capsule, respectively. Panels *1B* and *1E* are FLAIR and T1 images, respectively, of healthy controls.

2.2. Alternative Imaging Sequences and Image Analysis Tools

Apart from standard structural imaging sequences, many studies have examined sequences and analysis tools developed to explore other aspects of ALS pathology. Susceptibility weighted imaging (SWI) is used to image iron levels in imaged tissue. In the brain, abnormal iron deposits can cause inflammation, oxidative damage, and activation of microglia [Prell, 2015]. Increased iron levels have been known to occur in a number of neurodegenerative diseases including Alzheimer's, Parkinson's, and ALS [Mittal, 2009]. One study of SWI in ALS patients detected abnormal iron levels along the CST from the precentral gyrus to the posterior limb of the internal capsule [Prell, 2015]. Furthermore, these detected iron abnormalities were seen in other white matter structures including the corpus callosum and the superior longitudinal fasciculus [Prell, 2015]. One additional study demonstrated that abnormal iron levels can also be detected the motor cortex [Yu, 2014].

Another imaging sequence that can be used to examine pathology in the brain is diffusion weighted imaging (DWI), or its derivative diffusion tensor imaging (DTI). Diffusion imaging works on the premise of examining the diffusion of water molecules in the WM of the brain. Measured changes in diffusion properties can be indicative of pathological degeneration of WM structures. Some diffusion metrics of particular interest are fractional anisotropy (FA), axial diffusivity (AD), and radial diffusivity (RD). FA measures how unidirectional water diffusion is while AD and RD measure diffusion parallel to and perpendicular to the main direction of diffusion, respectively. FA can be linked to various pathological processes, but decreased AD is thought to be related to axonal degeneration and increased RD has been linked to a loss of myelin in the WM [Alexander, 2007]. In ALS patients, a number of studies have reported decreased FA and increased RD along the CST [Prudlo, 2012; Masuda, 2016; Bastin, 2013;

Muller, 2016; Sarica, 2017]. Cardenas-Blanco et al. (2016) also state that FA was able to strongly demonstrate disease progression in ALS with FA being highly influenced by RD values. Studies using DTI in ALS have used both deterministic and probabilistic tractography, with both demonstrating degeneration in the CST as well as other WM structures such as the stria terminalis, corpus callosum, and the subcortical WM of the caudate [Prudlo, 2012; Masuda, 2016; Bastin, 2013; Muller, 2016; Sarica, 2017; Cardenas-Blanco, 2016; Lillo, 2012].

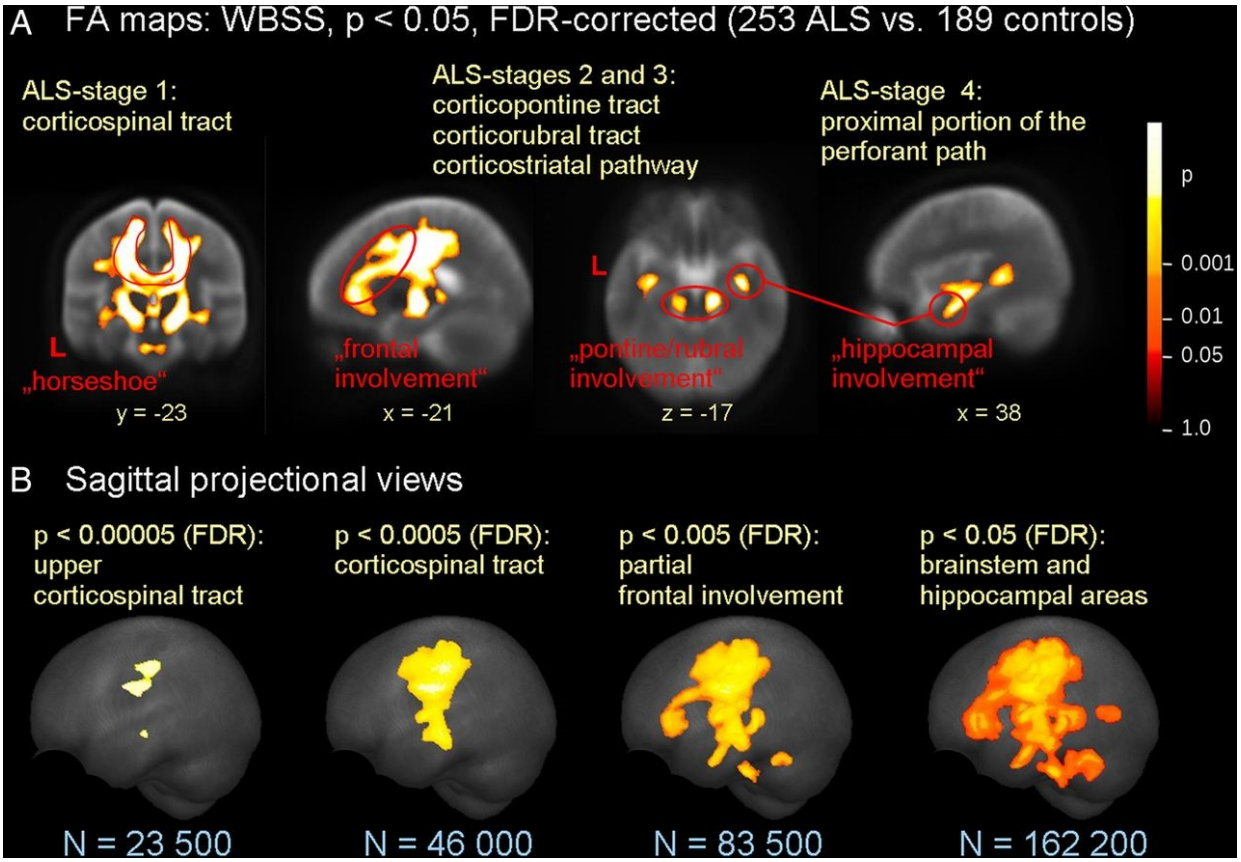

Figure 7. Significant areas of WM degeneration as detected by large multicentre study of diffusion imaging in ALS – taken from Muller et al. (2016).

While diffusion imaging techniques are used to examine WM in the brain, voxel-based morphometry (VBM) and cortical thickness are used to study the GM. Cortical thickness is self-explanatory, but VBM can measure either GM density or volume – though the default is

typically density. Significant reductions in both GM density and volume have been reported in the motor cortex of ALS pure patients [Rajagopalan, 2014; Devine, 2015; Bede, 2013]. Furthermore, this detected GM degeneration is more diffuse and moves into frontotemporal regions such as the prefrontal and orbitofrontal cortices, and the temporal poles in cases of patients with cognitive impairment [Rajagopalan, 2014; Kim, 2017; Masuda, 2016; Lillo, 2012; Chang, 2005]. Kim et al. (2017) examined differences in GM reduction based on onset type and found that bulbar onset patients showed a similar pattern of distribution, though their atrophy was more severe. Cortical thickness studies have been inconsistent in detected degeneration, but several have noted significant reductions of cortical thickness in the motor cortex of ALS patients [Rajagopalan, 2014; Rajagopalan, 2015]. These analysis tools are useful in the examination of patterns of GM and WM degeneration in ALS patients, but they have yet to be refined as methods to accurately and consistently differentiate ALS from mimic diseases. Thus, they cannot yet be considered as biomarkers for ALS. VBM, cortical thickness and DTI are also limited by their examination of only one tissue type at a time.

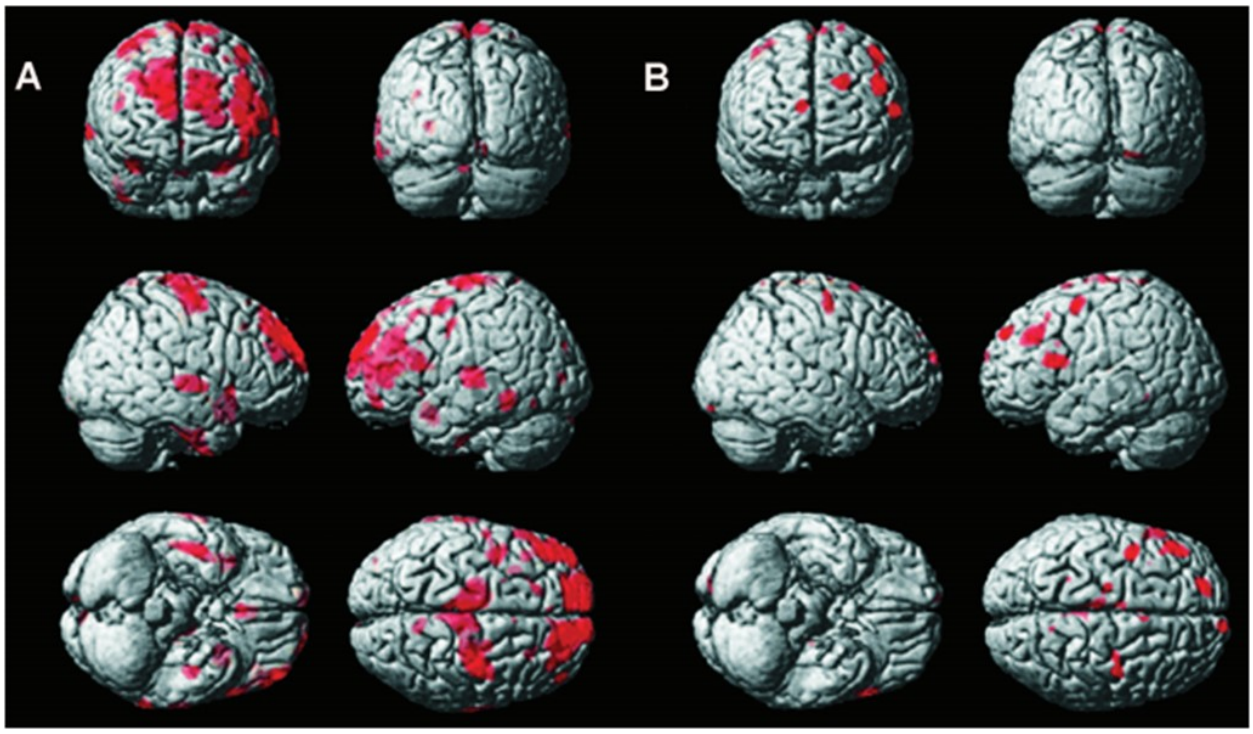

Figure 8. Areas of significant reduction in GM volumes for ALS and ALS-FTD patients – taken from Chang et al. (2005). Red regions are representative of significant patient-control differences.

In addition to these analysis tools for structural imaging sequences, other studies have looked to functional MRI (fMRI) in order to examine degeneration in the brain. Cerebral degeneration in fMRI would be measured as a disruption of functional networks such as the default mode network (DMN). Chio et al. (2014) examine the results of papers targeting resting-state fMRI. They detail several accounts in which there is altered connectivity in sensorimotor network, and extra-motor networks related to cognition and behaviour (2014). During task-based paradigms ALS patients demonstrate increased recruitment of premotor and supplementary motor areas for the same types of tasks – likely to compensate for degeneration of the motor cortex [Chio, 2014]. In addition to motor tasks, activation is altered during tasks related to language, executive function, and normal social-emotional function [Chio, 2014; Abrahams, 2004; Lulé, 2007].

One further MRI-based tool used to examine the brain in ALS patients is proton magnetic resonance spectroscopy (^{1}H-MRS), which examines the levels of metabolites in the brain. These metabolites can be indicative of neuronal health, as well as possible imbalances leading to pathology. MRS results have been variable in previous literature. Rooney et al. (1998) found NAA/(Cho+Cr) ratio to be reduced in the motor cortex, as well as the centrum semiovale and the internal capsule in the CST. Furthermore, they found that the ratio reductions in the motor cortex to be correlated with maximum finger tapping [Rooney, 1998]. Sivák et al. (2010) found significant differences in NAA/Cr ratio in the precentral gyrus, though no significant differences elsewhere or using other metabolite ratios. They make reference to a study by Chan et al. (1999) in which patients with purely UMN pathology (PLS) or more advanced ALS would present with reduced metabolite levels in the motor cortex. In contrast, patients with purely LMN syndromes did not show any significant differences [Chan, 1999]. Sivák et al. (2010) suggest that a lack of change in metabolite levels in ALS patients could be due to a mixed syndrome which hasn't yet progressed to substantial UMN involvement.

A final type of imaging used as a marker of degeneration in ALS is radiotracer-based imaging which includes both positron emission tomography (PET) and single-photon emission computed tomography (SPECT). F-fluorodeoxyglucose (F-FDG)-PET can be used as part of the diagnostic process of ALS and has been proposed as a diagnostic biomarker [van Es, 2017]. In ALS patients, there is a widespread decrease in glucose metabolism which affects areas including the motor cortex, extra-motor regions of the cortex, and the basal ganglia [van Es, 2017; Chio, 2014]. Furthermore, studies have noted hypermetabolism in the brainstem which could be indicative of reactive astrogliosis surrounding degenerating descending motor tracts [van Es, 2017; Chio, 2014]. Tanaka et al. (1993) examined oxygen metabolism using ^{15}O-PET

and found that cerebral oxygen metabolism was reduced in ALS patients compared to controls, though it was not statistically significant. However, they found that this hypometabolism was significant in the frontal and temporal lobes of patients suffering from comorbid dementia when compared to patients with only motor degeneration (Tanaka, 1993). Abe et al. (1993) performed a study using SPECT to examine the extent of cerebral degeneration in ALS and how that corresponds to cognitive impairment. They determined that patients with greater spatial extent of reduced metabolism as measured by SPECT – hypometabolism moving into frontotemporal regions from the motor cortex – corresponded with patients who had greater cognitive impairment [Abe, 1993].

2.3. Texture Analysis

Texture Analysis is an image analysis tool which was developed initially for pattern recognition in aerial landscape photos [Darling, 1968; Kassner, 2010]. However, more recently the scientific community has regained interest in texture as a means to assess medical images. Texture itself is traditionally defined as the feel or consistency of an object. However, in the context of imaging, texture is a quantification of the regional relationships of grey level intensities in an image. Intensity is simply how bright or dark a given pixel (2D) or voxel (3D) is. In medical imaging, the raw intensity value is indicative of the type of tissue being imaged, or it can also indicate the presence of pathology as seen in structural imaging studies [Maggi, 2018; Rashid, 2008; Hecht, 2001; Keller, 2010]. However, visual assessment of image intensities relies on a certain level of subjectivity. This subjectivity is theoretically eliminated with texture calculation based on intensity values. Different texture features are calculated using mathematical equations which consider grey level homogeneity, contrast, and a number of other qualities within a set radius from a seed point. In a medical image, each pixel or voxel acts as a

seed for these calculations. There have been a number of different methods for texture calculation.

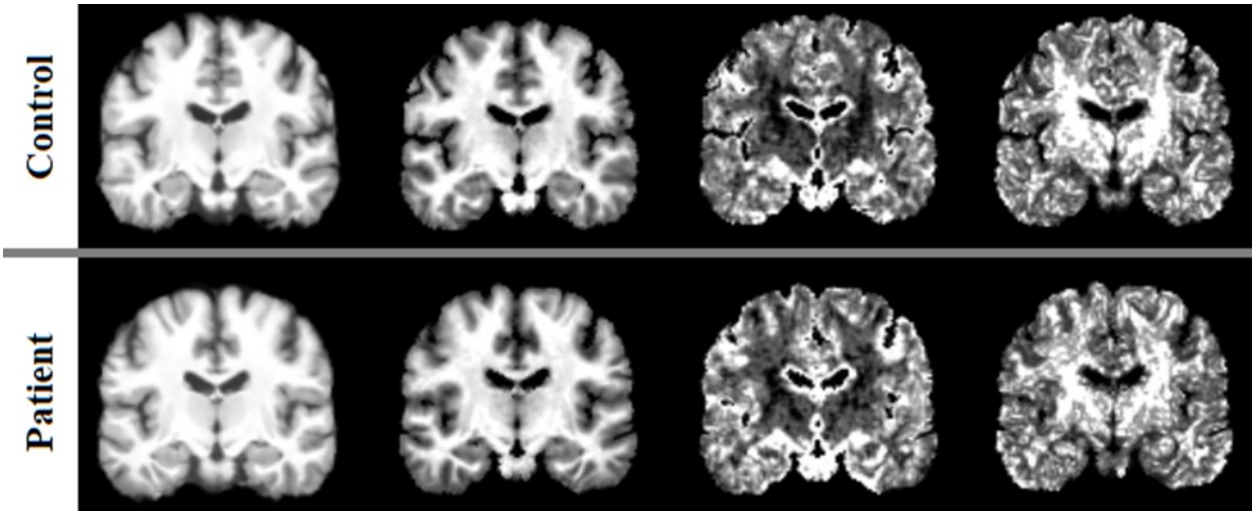

Figure 9. Demonstration of how T1 images are altered visually by calculation of various texture features. Top images are of a single control, and bottom images are of a single patient. From left to right, both rows consist of a T1-weighted image and texture features *autoc*, *contr*, and *energ*, respectively. Differences are difficult to see on visual inspection, though they are most visible in the CST.

Kassner (2010) details the three most common forms of texture features, the first of which being syntactic texture features. Syntactic features identify "fundamental elements of the image, which are then linked through syntax," and while there are potential applications to brain volumetry and surface mapping there has been little use in medical imaging [Kassner, 2010]. Spectral features are another one of these feature types and are used primarily to detect larger scale or coarse changes in an image [Kassner, 2010]. The final type – also the most popular and successful among medical imaging studies – is statistical features which are inclusive of first order features (ex. MGL and VGL), and second order features which are extracted from grey level co-occurrence matrices (GLCM) or run length matrices (RLM) [Kassner, 2010; Maani, 2015]. GLCMs work by tabulating grey level values in a matrix and calculating various interrelationships between those intensity values, whereas RLMs work by calculating the number

of times the same intensity value occurs in a row along a vector moving away from a seed point [Kassner, 2010]. Both of these can be useful in examining how brain tissue can change with pathology, as they can detect even slight variations in how neighbouring pixels and voxels appear in relation to each other.

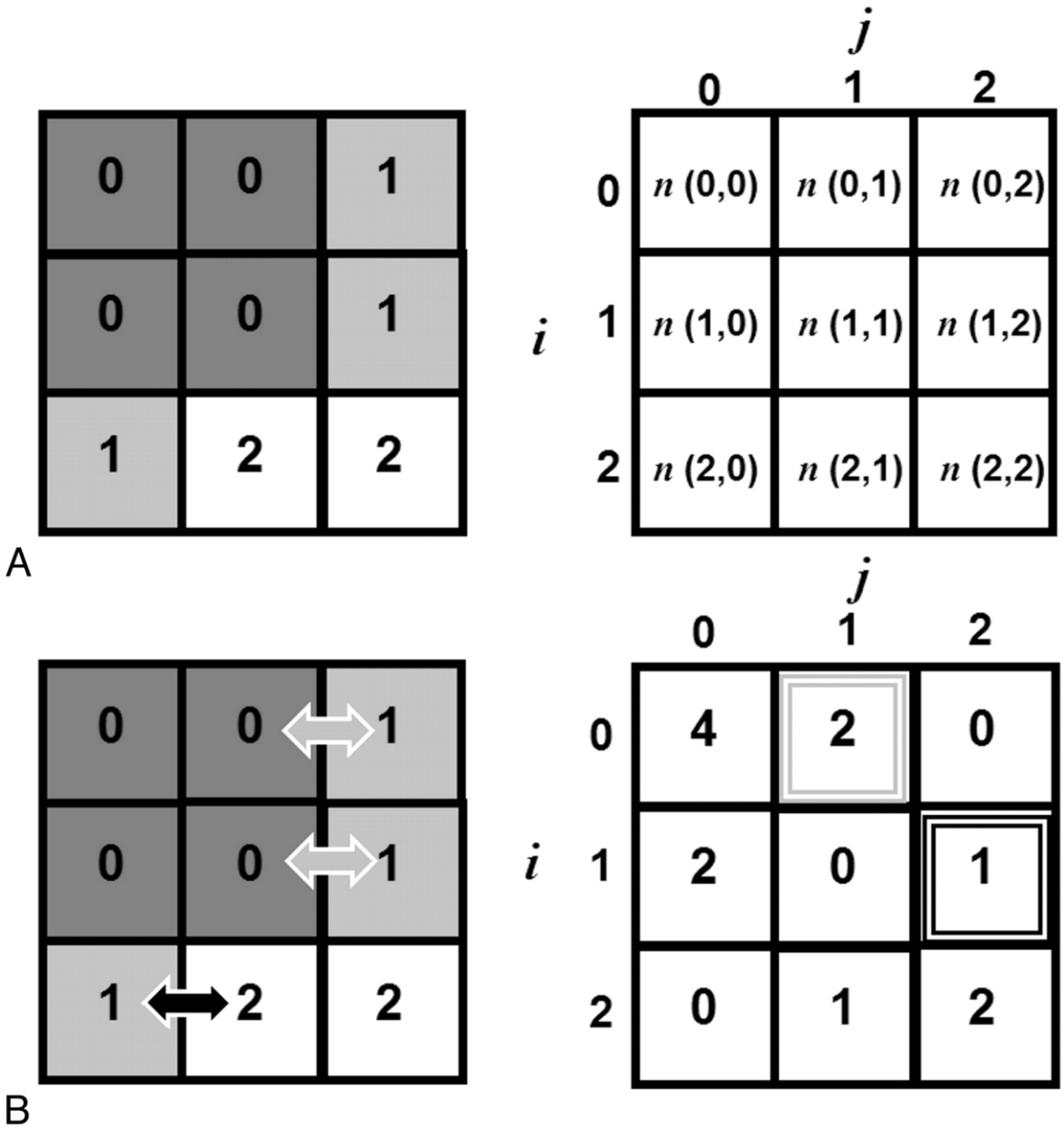

Figure 10. Graphic representation of a basic 3x3 GLCM design – taken from Kassner and Thornhill, (2010).

GLCM features have been used to examine cerebral pathology for a number of different conditions. Bonhila et al. (2003) used MAZDA software to examine hippocampal sclerosis in medial temporal lobe epilepsy patients. They determined that TA of FLAIR images detected this sclerotic pathology using nearly all of the features examined, and that this detected pathology was consistent with histological evidence for each patient [Bonhila, 2003]. Additionally, Sankar et al. (2008) implemented TA as a means to study different tissue properties in temporal lobe epilepsy patients. They determined that TA was more sensitive than conventional MRI visual assessment and volumetry for the detection of pathological signs such as temporopolar blurring [Sankar, 2008]. Further applications in epilepsy include work by Antel et al. (2003) who were investigating GLCM-based texture abnormalities associated with focal cortical dysplasia (FCD). Based on their analysis, the GLCM features were able to detect pathological lesions with 83% sensitivity, compared to a 61% sensitivity by a standard visual assessment [Antel, 2003]. While neither method resulted in misclassification – 100% specificity in both cases – an increased sensitivity is useful in presurgical planning to help control the condition [Antel, 2003]. TA has also been applied in the differentiation of glioblastoma phenotypes. Chaddad and Tanougast (2016) performed GLCM-based TA on T1 and FLAIR images to determine whether texture is indicative of phenotype and survival. They found that each of 22 examined texture features detected significant differences between phenotypes, and they were able to discriminate with high sensitivity and specificity [Chaddad and Tanougast, 2016]. Furthermore, seven of these features were predictive of survival for each respective phenotype [Chaddad and Tanougast, 2016].

Neurodegenerative disorders have also previously been a target of study using TA. Sikio et al. (2015) used four texture features in MAZDA to look at patterns of cerebral degeneration

associated with Parkinson's disease, and how longitudinal texture changes are associated with clinical measures of disease progression. They found significant differences in patients located in areas including the substantia nigra, the pons, and the basal ganglia [Sikio, 2015]. Additionally, they determined that longitudinal change was present in the thalamus and basal ganglia, and that texture changes correlated with MMSE and UPDRS scores [Sikio, 2015]. Dementia has also been a point of interest for TA. Oppedal et al. (2015) used local binary pattern (LBP) texture features for classification of Lewy Body dementia and Alzheimer's disease. Performance was relatively good with classification as accurate as 0.74 when only factoring in the two, and 0.87 when also factoring in healthy controls [Oppedal, 2015]. Sørensen et al. (2016) used hippocampal texture as a classifier for early detection of Alzheimer's disease. Support vector machine was able to differentiate AD from healthy controls with an AUC of 0.912, and MCI from control at 0.764 [Sørensen, 2016]. Furthermore, when combined with hippocampal volume this classification improved to 0.915 and 0.806, respectively, lending support to both texture itself and a multimodal approach to diagnosis [Sørensen, 2016]. In addition to these classifications, TA has been used to study patterns of cerebral degeneration associated with AD noting significant pathological change spreading outward from the hippocampus [Maani, 2015]. Other neurodegenerative disorders targeted include Huntington's disease and MS. Doan et al. (2014) used GLCM texture features to assess cerebral change associated with Huntington's disease, and found significant texture abnormalities localised to the basal ganglia, thalamus, and hippocampus. They further noted that there were significant texture abnormalities present in premanifest patients, indicating TA's ability to detect cerebral change before manifestation of symptoms [Doan, 2014]. In the case of MS, studies have looked at TA's ability to assess pathological lesions in the brain. Early works by Yu et al. (1999) determined that TA had the

ability to define whether or not a lesion was active with high sensitivity and specificity. TA's success here is important as its implementation to identify active lesions would minimize use of gadolinium injections [Yu, 1999].

ALS, thus far, has only been studied twice in published works using texture. de Albuquerque et al. (2016) used a 2D, ROI-based approach to study pathological change in the deep grey nuclei. The study sample was made up of 8 bulbar onset and 25 limb onset patients, and they used eleven GLCM-based texture features for their analysis [de Albuquerque, 2016]. This analysis found significant patient-control differences to be located bilaterally in the thalamus, and in the right caudate. They also used texture as a classifier for ALS patients versus controls to relatively good success with peak performance being 81.25% sensitivity and 56.25% specificity. The other study of ALS patients was a 3D whole-brain analysis of GLCM features as a measure of cerebral degeneration [Maani, 2016]. Of four features calculated, all detected significant texture abnormalities in the precentral gyrus and the CST, and two features detected additional changes in the cingulum, thalamus and hippocampus [Maani, 2016]. The texture abnormalities detected had high sensitivity and specificity – the best of which having AUC values greater than 0.9 [Maani, 2016]. Additionally, feature *Svar* in the right CST correlated negatively with right-hand finger tapping, and all features correlated negatively with symptom duration [Maani, 2016]. Both of these previous studies in ALS as well as applications to other pathological processes provide promising evidence for TA being an effective and objective measure of disease presence and progression.

3. Rationale for Thesis

As previously described, ALS is a highly heterogeneous and aggressive degenerative disorder. The current diagnostic process is long and complicated. Not only would a biomarker for ALS facilitate diagnosis, but an earlier diagnosis will also allow for earlier initiation of drug trials when the pathological process is potentially more amenable to treatment. Furthermore, biomarkers allow for the tracking of disease progression, thereby allowing for an objective measure of whether or not a drug trial is offering any improvement in the patient's condition. An earlier diagnosis would also allow for a more rapid implementation of any treatment with the goal of improving patient quality of life. TA holds promise as a potential biomarker of cerebral degeneration in ALS. Previous studies using TA have examined different diseases including temporal lobe epilepsy, Alzheimer's disease, and glioblastoma, all showing a strong discrimination between patients and controls or pathological phenotypes [Bonhila, 2003; Antel, 2003; Sikio, 2015; Oppedal, 2015; Sørensen, 2016; Chaddad and Tanougast, 2016]. In addition, TA has been applied to ALS in two previous studies. One of these studies examined deep grey structures using a 2D, ROI based analysis [de Albuquerque, 2016], and one examined cerebral degeneration using a 3D, whole-brain analysis [Maani, 2016]. Both of these studies report that TA was excellent in terms of its ability to differentiate between patients with ALS and controls [de Albuquerque, 2016; Maani, 2016]. The present study looks to examine cerebral degeneration in ALS and replicate previous findings using data collected prospectively from multiple centres. A major benefit of TA is that it uses routine clinical scans that are acquired during the diagnostic process of the disease. These routine scans typically show few differences between ALS patients and healthy controls. However, as has been shown in previous studies, TA effective at examining cerebral degeneration in both GM and WM structures [de Albuquerque, 2016; Maani, 2016].

One of the major goals was to examine areas of degeneration as detected by texture abnormalities in a cross-sectional analysis, both in areas of known pathology such as the precentral gyri and the corticospinal tracts, but also in areas that may not be expected. In addition to this, the present study aimed to show that TA is a reliable and objective measure regardless of the site of acquisition – or more specifically, the scanner used to acquire the images. This project hoped to examine patterns of cerebral degeneration primarily using a pooled sample from all sites of acquisition, but also to look at these sites individually. Finally, this project hoped to examine the relevance of any detected degeneration to the overt impairment seen in clinic. To do this, extracted texture values were compared with clinical measures of degeneration such as finger and foot tapping scores.

The hypotheses for the thesis project as a whole were as follows:

1. TA will detect cerebral degeneration in ALS patients when compared to controls.
2. Texture abnormalities will be present in pathologically relevant GM and WM regions of the brain including both motor and extra-motor areas.
3. Texture is a reliable and reproducible measure between sites of acquisition.
4. Texture abnormalities will be consistent across all sites of acquisition in cross-sectional analyses.
5. Detected pathology in motor regions of the brain will correlate with clinical measures of disease-related impairment.

4. Preliminary Analyses

4.1. Optimising Pipeline

The initial stage of data analysis involved a large amount of troubleshooting. A major consideration in the processing pipeline was that each step was tailored to use with a particular version of their respective software. The software versions present on the computer I was using were not consistent with those that were ultimately required. This led to some processing mismatches. The most significant of these issues was a mismatch in preprocessed files, masks, and the deformation fields used to subsequently normalise the texture maps into MNI space. The automation of the mask creation process was run using a batching script in Python. However, the script was written for a different version of the software than the version running on my computer, leading to an issue in properly executing the task. This subsequently led to improper pairing of masks with bias corrected images meaning that texture feature extraction was performed in the masked space of the wrong subject. This mismatch presented as diffuse abnormalities throughout the whole brain. Most peculiarly, there was a very large cluster group around the base and outside of the cerebellum, and the rest of the results carried no biological validity to them. Because of this mismatch, texture calculations for a number of subjects included ventricular space and areas outside the brain. The mismatch was rectified by uninstalling all the software, and subsequently reinstalling the versions required.

4.2. Refining Analysis Techniques

Subsequent processing of data was more successful with the results showing significant texture differences between ALS patients and controls in pathologically relevant areas. Cross-sectional group comparisons of each of the individual sites were run, as well as a pooled analysis of subjects from all sites. These were both carried out using 2-sample t-tests which took into

account participant age as a covariate so as to remove any confounding texture abnormalities that were present due to normal, healthy aging processes. Texture abnormalities were variable between sites of acquisition with significant patient-control differences occurring in the CST, the PCG, and several other GM and WM structures throughout the brain. Results here were more promising and demonstrated changes that were relevant to the disease based on accepted literature.

4.3. Tuning Inter-Site Corrections

After ensuring that the processing pipeline was working properly, I decided that it would be important to correct for differences between sites of image acquisition. This was added into the t-test analysis as a covariate in the pooled-samples model alongside participant age. It wasn't possible to add a categorical variable in as a factor in the t-test, so it was added here as a continuous value – each site having its own value from 1-4. The addition of this controlling factor helped to remove some of the noise present in the previous version of the analysis.

However, it was subsequently decided that in order to ensure proper statistical protocol, site of acquisition needed to be controlled for by way of a full factorial model. Thus, the pooled sample cross-sectional analysis was rerun using a full factorial analysis that included site of acquisition and diagnosis as the main factors of the analysis. In addition to this, age and brain parenchymal fraction (BPF) were included as covariates. BPF is recognised as a measure of global brain atrophy and is calculated as the ratio of the combined GM and WM volumes to the total intracranial volume. It was thought that controlling for BPF in this analysis would allow for us to examine change in the brain that is not associated with atrophy. Following this adjustment to the statistical model, BPF was added as a covariate for each site's individual analysis as well.

4.4. ACPC Realignment

The final adjustment made to the processing pipeline was realignment to ACPC orientation. Despite this being the desired orientation for the images upon acquisition, a number of them were off to some degree. Normally this issue would be resolved by registration in analyses such as VBM. However, due to the fact that TA is calculated in the image native space within a matrix of predefined orientation, it becomes necessary to ensure as much consistency in image alignment prior to actual processing. Therefore, this realignment was added onto the analysis for each individual as the first step of processing after conversion of the raw DICOM images to Niftii format.

4.5. A-Priori ROI Correlations

One of my initial hypotheses involved the correlation of texture changes in specific structures of known pathology in ALS. These structures were the precentral gyri and the corticospinal tracts. These structures were selected from a literature-based train of reasoning that pointed toward this type of focal pathology. FSL was used to extract masks of these two structures with atlases as a guide. The CST masks were created with the Jülich Histological Atlas and the precentral gyrus masks were extracted from the Automatic Anatomical Labelling (AAL) brain atlas. These masks were extracted both unilaterally (L and R individually) and bilaterally. These masks were created slightly larger than the structure of interest to control for mild individual differences in the MNI space. However, the CST and PCG masks were subtracted from each other to ensure no overlap of GM and WM in the extracted values. This was done with the understanding that GM and WM might behave differently in texture calculations, and any overlap of these areas should be mitigated prior to analysis. Seven features were examined in this analysis. The values extracted from these ROIs were analysed using partial correlations to

control for both age and site in the model. Correlations with contralateral finger tapping, contralateral foot tapping, UMN total score, ALSFRS-R, and BPF were examined. Results here were deemed to be significant at $P<0.05$.

The results of this analysis showed that two of the seven calculated texture features were significantly correlated with either contralateral finger tapping or contralateral foot tapping. No features significantly correlated with UMN burden total score in the examined ROIs. However, five features correlated with BPF in at least one ROI. No ROIs correlated significantly with ALSFRS-R in the pooled sample. The results are summarised in Table 1. It was decided after this analysis that using an ROI created based on any significant differences discovered by the full factorial model in the motor regions of the brain would be more representative of the objectives of the project. The hypothesis that this decision was based on was that the detected areas of significant change in the large sample would be more representative of the pathology contributing to any clinical measure of UMN degeneration.

Table 1. Significant correlations between pooled-sample texture feature values and clinical measures of disease severity. Correlations between texture feature values and clinical measures of finger tapping, foot tapping, and UMN burden, and BPF are shown. Seven features were examined in an ROI-based analysis of the precentral gyri (PCG), the corticospinal tracts (CST). Tapping scores were examined in comparison with texture in contralateral structures (eg. Right finger tapping with Left PCG) while UMN burden and BPF were compared to bilateral ROIs.

Correlate	Feature	ROI	(n)	P-value	Correlation coefficient (r)
Contralateral finger tapping	*autoc*	PCG	112	0.0474	0.191
	cprom	PCG	112	0.0060	0.262
Contralateral foot tapping	*cprom*	PCG	100	0.0478	0.203
BPF	*corrp*	PCG	64	0.0274	0.285
	cprom	CST	64	0.0273	-0.285
	cshad	PCG	64	0.0491	0.255
	energ	PCG	64	0.0021	0.390
	indnc	CST	64	0.0021	0.390
		PCG	64	<0.0001	0.670

4.6. Controlling for Site, Scanner, or Both

One of the major considerations in the analysis was how to correct for image acquisition at multiple sites. Studies suggest that multicentre data acquisition with MRI can be prone to significant differences due to hardware differences [Takao, 2013; Focke, 2011]. In the acquisition of data for the present study, two different scanner platforms were used. For this reason, it was important in the analysis to do everything possible to control for any effect of scanner difference. The initial thought was that controlling for site of acquisition would be the most careful way of examining the effect of diagnosis. However, given that this study is examining patients with ALS – a notoriously heterogeneous disease – it was thought that controlling for MRI scanner platform might be an accurate way of controlling for acquisition

differences while minimising effects of heterogeneity. Based on glass brain representation, the results are marginally different when controlling by site compared to controlling by scanner platform. It was then thought that perhaps to be the most mindful of these differences, it would be best to control for both scanner and site. When this analysis was run as a test, the results were identical to those controlling for only site for all features calculated. This suggests that results controlling for site rather than scanner platform does in fact also account for any variation introduced even by scanners of the same model. Controlling for site was selected as the course of action moving forward for all aspects of the analysis. Results are shown below in Figure 11.

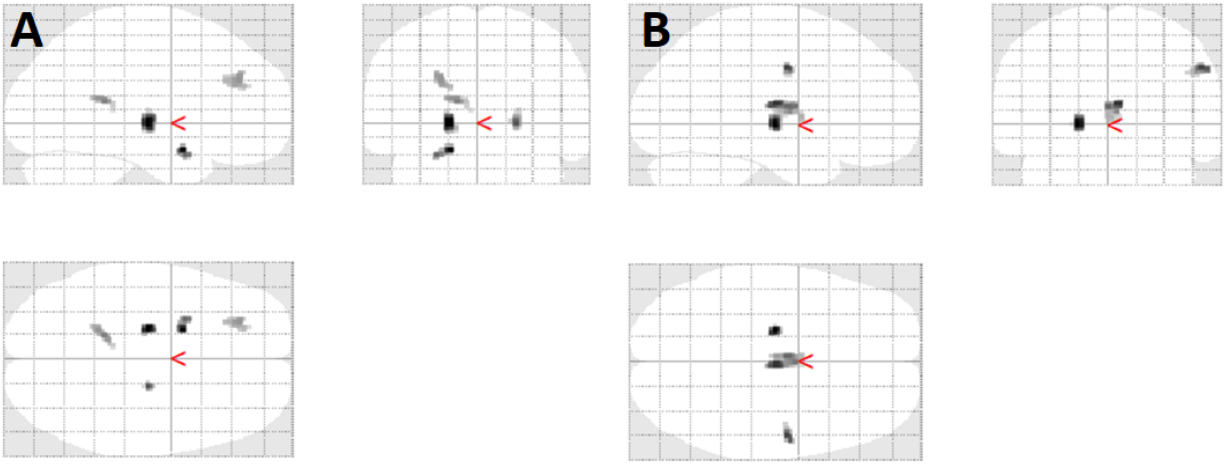

Figure 11. Glass brain representation of feature autoc controlling for site of acquisition (A) and scanner platform (B). Noteworthy differences between the two analyses are seen in the right internal capsule, the middle frontal gyrus, and Brodmann area 28 in A, and the precentral gyrus and thalamus in B. Results controlling for both site of acquisition and scanner platform were identical to those controlling for only site (A).

5. Experiment 1: Travelling Heads Reliability

5.1. Introduction

The reliability of 3D TA has not been adequately tested in previous literature. Few studies have previously evaluated the reproducibility of TA results, though a handful have examined the effects of scanner and scanning parameters on TA's ability to differentiate between different textures in foam phantoms [Lerski, 1999; Mayerhoefer, 2009; Waugh, 2011]. These studies have reported mixed results, though they have reported that GLCM features are often relatively robust compared to other categories of texture features [Lerski, 1999; Mayerhoefer, 2009; Waugh, 2011]. Previous studies have also only examined 2D TA. The present study looks to examine the reliability and reproducibility of 3D texture features both within and between sites of image acquisition using a harmonised data acquisition protocol. Furthermore, the present experiment looks to test the reliability of TA on human subjects which means it is more generalizable to future works examining effects of disease. Showing that texture is consistent both within and between sites of acquisition provides greater support for its implementation in larger scale multi-centre studies. Furthermore, examination of reliability on a multi-centre scale is an important step in the validation of TA as a biomarker prior to implementation in a clinical setting in which images will be acquired on different hardware at each centre.

5.2. Materials and Methods

5.2.1. Study Participants

6 healthy subjects (4 male, 2 female) were recruited from the University of Alberta to participate in the study. To be included in the study, participants had to have no history of neurological or psychiatric conditions, nor could they have had any prior history of a head injury.

Subjects were scanned at five sites across Canada: Edmonton – Peter S. Allen MR Research Centre, Calgary – Seaman Family MR Research Centre, London – Robarts Research Institute, Montreal – Montreal Neurological Institute, and Toronto – Sunnybrook Research Institute. At all sites of acquisition, two scans were performed on the same day for each subject (~1 hour apart).

5.2.2. MRI Acquisition Protocol

Scans were acquired at all sites on clinical research MRI systems operating at 3 T: Siemens Prisma (Erlangen, Germany) in Edmonton, Siemens Trio (Erlangen, Germany) in Montreal, and General Electric MR750 (Milwaukee, WI) in Calgary, London, and Toronto. It was targeted to scan with the same spatial parameters at each site of acquisition to produce images optimized for signal to noise ratio (SNR) and contrast to noise ratio (CNR) despite different scanner models and manufacturers. 3D T1 scans were acquired using MPRAGE sequence on Siemens scanners (TR = 2300 ms, TE = 3.43 ms, TI = 900 ms, flip angle = 9°, FOV = 256 × 256 mm, resolution = 1 mm × 1 mm × 1 mm), and using FSPGR on GE scanners (TR = 7400 ms, TE = 3.1 ms, TI = 400 ms, flip angle = 11°, FOV = 256 × 256 mm, resolution = 1 mm × 1 mm × 1 mm).

5.2.3. Data Preprocessing

Data were converted from raw DICOM format to Niftii files using dcm2nii converter (MRIcron). These files were then realigned to ACPC orientation using an automation script called acpc_coreg running in SPM12. The data were subsequently modulated, segmented into grey and white matter, and bias corrected using the high dimensional DARTEL algorithm in the VBM8 toolbox of SPM8 (http://www.fil.ion.ucl.ac.uk/spm/). During this step, deformation fields were also created for subsequent normalization of texture maps into MNI standard space.

5.2.4. 3D Texture Analysis

The binarized GM and WM segments created in the VBM preprocessing were used to create a mask of each subject's brain in its own native space. The masks were created including the GM and WM regions so as to exclude ventricular regions in each brain. These masks were created using the image calculator tool in SMP8. Texture analysis was run using VGLCM TOP3D [Maani, 2015], a toolbox developed in our lab that is also run through SPM8. The input for this toolbox is the modulated, bias corrected image for each subject, and their respective binary mask created from the segmented GM and WM images. Texture feature extraction is done using the mask as a guide for what to include in the calculated area of the brain. Each voxel is used as a point of origin for its respective texture value. The texture value calculation is done with a neighbourhood radius of 1, a distance of 1, and a quantization level of 8.

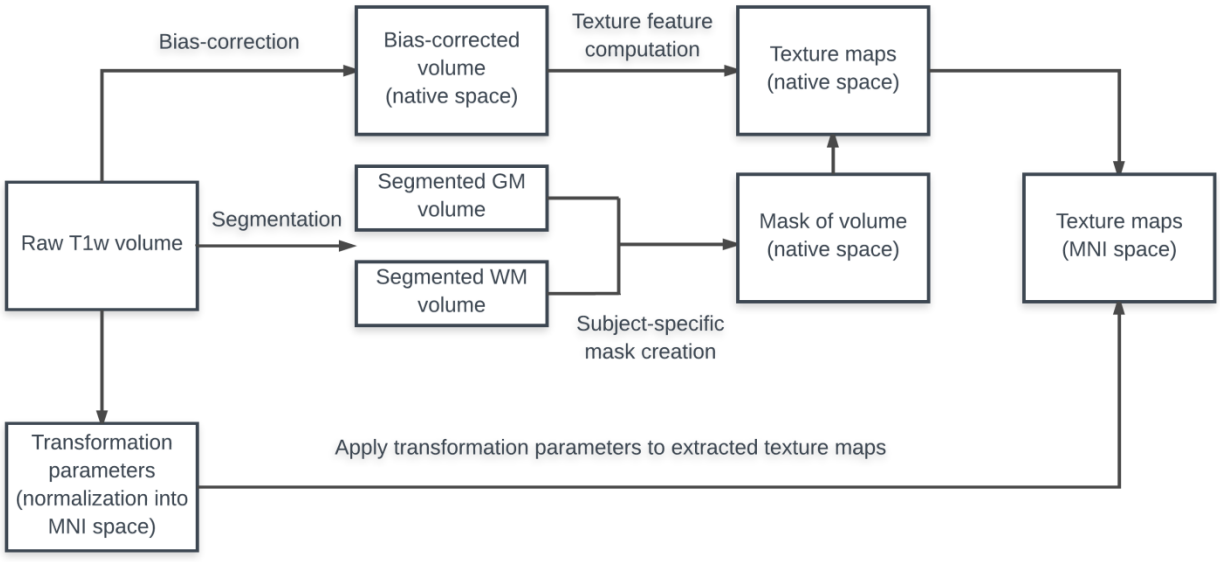

Figure 12. Image processing pipeline for 3D texture analysis.

Each feature is calculated at every voxel included in the mask in the axial, sagittal, and coronal planes relative to the voxel of origin, and these values are then averaged to represent the

value for that three-dimensional voxel space. These calculations are done in the native space of each brain, and they are subsequently warped to the MNI152 standard space using the deformation fields created during preprocessing steps.

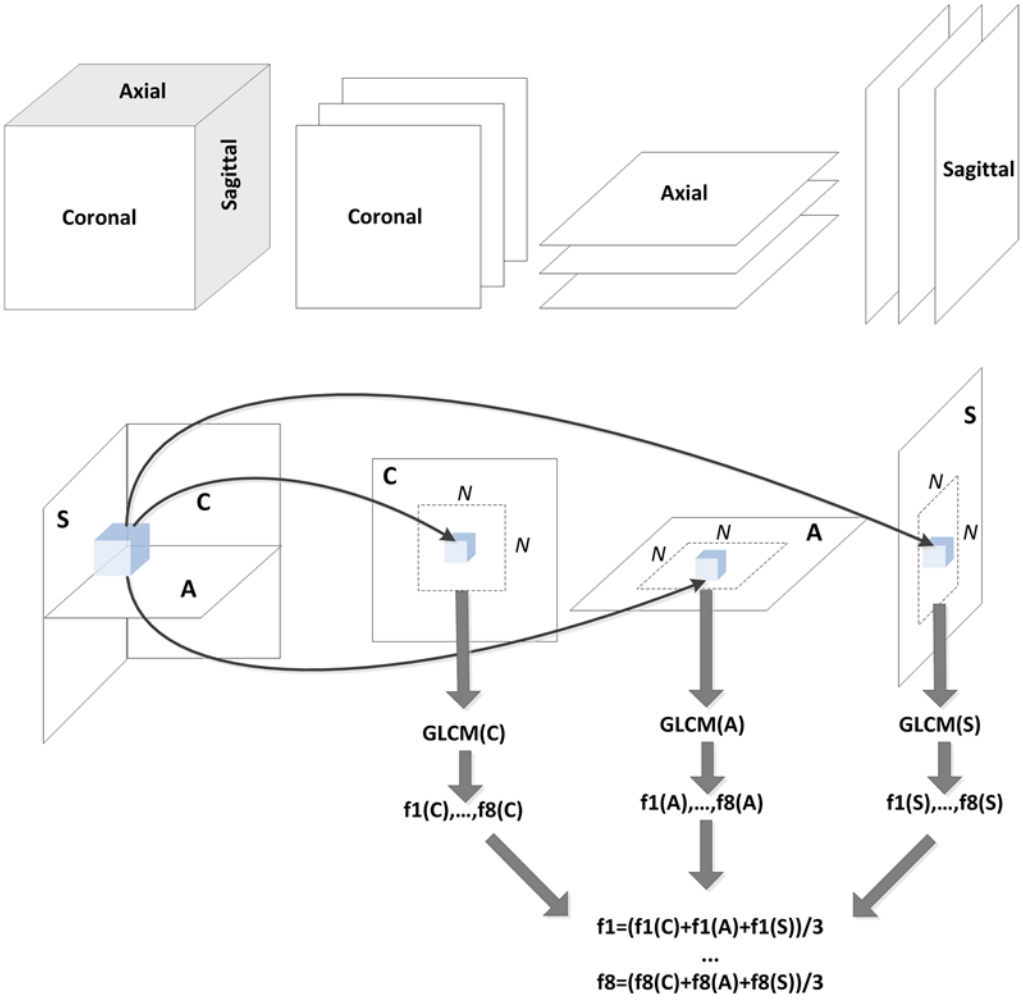

Figure 13. Graphic representation of feature calculation using VGLCM TOP3D toolbox, taken from Maani et al. (2015).

The toolbox consists of 22 different texture features from which 7 were chosen as non-redundant. This selection was done by correlating the calculated feature values and removing one from any pair of features that correlated with a coefficient of greater than 0.9. The calculated features for this analysis included Autocorrelation (*autoc*), Contrast (*contr*), Correlation (*corrp*),

Cluster Prominence (*cprom*), Cluster shade (*cshad*), Energy (*energ*), and Inverse Difference Normalised (*indnc*). A brief description of each feature is included in Table 2.

Table 2. Description of texture features calculated in the present study. Information was extracted from various sources [Yang, 2012; Shapiro and Stockman, 2000; Maani, 2015].

Feature	Abbreviation	Formula	Meaning
Autocorrelation	*autoc*	$f_1 = \sum_{i=1}^{G}\sum_{j=1}^{G}(ij)P(i,j)$	Measure of repetitive patterns of intensity in neighbouring voxels
Contrast	*contr*	$f_9 = \sum_{i=1}^{G}\sum_{j=1}^{G}\lvert i-j\rvert^2 P(i,j)$	Measure of similarity/contrast of intensity in neighbouring voxels
Correlation	*corrp*	$f_4 = \frac{\sum_{i=1}^{G}\sum_{j=1}^{G}(i-\mu_y)(j-\mu_x)P(i,j)}{\sigma_x\sigma_y}$	Measure of linear dependency of grey-level intensities on neighbouring voxels
Cluster Prominence	*cprom*	$Pro = \sum_{i=0}^{N_g-1}\sum_{j=0}^{N_g-1}\left(i+j-u_x-u_y\right)^4 p(i,j)$	Measure of image asymmetry and quantifies grey-scale variation
Cluster Shade	*cshad*	$Sha = \sum_{i=0}^{N_g-1}\sum_{j=0}^{N_g-1}\left(i+j-u_x-u_y\right)^3 p(i,j)$	Measure of matrix skew and asymmetry in neighbouring voxels
Energy	*energ*	$f_3 = \sum_{i=1}^{G}\sum_{j=1}^{G}P(i,j)^2$	Measure of image homogeneity in total number of calculated grey levels
Inverse Difference Normalised	*indnc*	$f_{10} = \sum_{i=1}^{G}\sum_{j=1}^{G}\frac{1}{1+(i-j)^2/G^2}P(i,j)$	Measure of local homogeneity in the pairing of grey levels in adjacent voxels

5.2.5. Anatomical ROI Extraction

Masks of twelve anatomical structures throughout the brain were created manually using FMRIB Library (FSL), guided by multiple atlases. The Jülich Histological Atlas was used to produce probabilistic masks of the amygdala, Broca's area, the hippocampus, and the corticospinal tract with a probabilistic threshold of 30%. The MNI Structural Atlas was used for a mask of the thalamus. Lastly, the AAL atlas was used to produce masks of the caudate, pallidum, putamen, precentral gyrus, postcentral gyrus, the cingulate cortex, and the orbitofrontal cortex. In addition to these structures, a whole brain mask was created using the MNI Structural Atlas to extract a whole brain average texture value. These masks were applied to the calculated texture maps to extract average values at each structure for each individual scan.

5.2.6. Statistical Analysis

Intra-class correlations (ICC) were examined as a measure of reliability and reproducibility of texture within and between sites of image acquisition. ICCs measure how strongly units in groups of the same measure resemble each other. ICCs were computed in MedCalc version 17.6 using a two-way mixed effects model. This was based on the assumption that the statistical effect of the rater is fixed and the effect of the ratee is random. They were calculated for each extracted ROI on each of the seven features calculated. To calculate scan-rescan reliability, each subject's scan 1 was grouped and each subject's scan 2 was grouped. To calculate inter-site reliability, all scans were divided into their respective sites of acquisition for a total of 5 groups.

5.3. Results

5.3.1. Scan-Rescan Reliability

Scan-rescan reliability was high for five of the seven features examined. Features *autoc*, *contr*, *cprom*, *energ*, and *indnc* had excellent agreement between measurements at most ROIs (ICC>0.7). In contrast, features *corrp* and *cshad* had lower reliability at most ROIs (ICC<0.5). Results are summarised in Table 3.

Table 3. Scan-rescan ICC values at all ROIs for each of seven texture features. Results indicate high reliability for five features (*autoc*, *contr*, *cprom*, *energ*, and *indnc*), and moderate to low reliability for two (*corrp* and *cshad*).

	autoc	*contr*	*corrp*	*cprom*	*cshad*	*energ*	*indnc*
Amygdala	0.8602	0.956	-0.6405	0.9286	0.3861	0.9689	0.9223
Broca's Area	0.8751	0.9752	-0.4231	0.9733	0.4398	0.9556	0.9805
Hippocampus	0.7361	0.953	-0.4693	0.9417	0.3884	0.977	0.9734
Cingulate Cortex	0.8984	0.9568	-0.2819	0.9661	0.4367	0.9634	0.9913
Postcentral Gyrus	0.9516	0.9829	-0.3427	0.9754	0.4653	0.9743	0.9948
Orbitofrontal Cortex	0.924	0.9333	-0.5521	0.9543	0.4159	0.8656	0.9667
Caudate	0.9622	0.9598	0.3789	0.9626	0.5754	0.969	0.9981
Pallidum	0.9114	0.969	-0.3882	0.952	0.3698	0.942	0.9586
Putamen	0.9538	0.9318	-0.535	0.9066	0.3708	0.9241	0.9331
Thalamus	0.9058	0.983	-0.4089	0.9677	0.3375	0.9825	0.993
Corticospinal Tract	0.9221	0.8822	-0.3653	0.9443	0.3707	0.8662	0.9253
Precentral Gyrus	0.9569	0.9758	-0.4366	0.9647	0.4359	0.9724	0.9847
Whole Brain	0.8435	0.9004	-0.476	0.939	0.3954	0.976	0.9812

5.3.2. Inter-Site Reliability

Inter-site reliability was high once again features *autoc*, *contr*, *cprom*, *energ*, and *indnc*. These features showed almost entirely excellent agreement (ICC>0.7) between measures at different sites of acquisition while features *corrp* and *cshad* showed mostly moderate to low agreement (ICC<0.5). Results are summarised in Table 4.

Table 4. Inter-site ICC values at all ROIs for each of seven texture features. Results indicate high reliability for five features (*autoc*, *contr*, *cprom*, *energ*, and *indnc*), and moderate to low reliability for two (*corrp* and *cshad*).

	autoc	*contr*	*corrp*	*cprom*	*cshad*	*energ*	*indnc*
Amygdala	0.9031	0.7211	0.1613	0.8335	-0.291	0.648	0.8533
Broca's Area	0.8224	0.8271	0.2927	0.7517	-0.4693	0.8927	0.9619
Hippocampus	0.5762	0.2759	0.2368	0.8072	-0.2613	0.7667	0.9721
Cingulate Cortex	0.9426	0.8103	0.3354	0.8386	-0.377	0.8537	0.9619
Postcentral Gyrus	0.9218	0.9322	0.3384	0.9193	-0.5501	0.8806	0.9813
Orbitofrontal Cortex	0.9419	0.8267	0.2179	0.8598	-0.3427	0.6404	0.9363
Caudate	0.9782	0.9664	0.7795	0.9847	-0.4894	0.936	0.9985
Pallidum	0.9138	0.8208	0.2028	0.8925	-0.293	0.8543	0.8533
Putamen	0.8883	0.9084	0.1954	0.9133	-0.2908	0.8386	0.8817
Thalamus	0.949	0.566	0.2047	0.3795	-0.2661	0.6393	0.9867
Corticospinal Tract	0.9345	0.8744	0.135	0.9333	-0.3088	0.882	0.8924
Precentral Gyrus	0.9139	0.8381	0.2972	0.8697	-0.4523	0.9261	0.9814
Whole Brain	0.8945	0.7674	0.1959	0.8136	-0.3518	0.9266	0.9678

5.4. Discussion

The results of this experiment indicate that several of the texture features are highly reliable and reproducible both within and between sites of image acquisition. Few studies have been previously done testing the reliability of texture analysis. Those that have been done have all used foam phantoms as a measure of reliability [Lerski, 1999; Mayerhoefer, 2009; Waugh, 2011]. These studies examined TA's reliability in discrimination of these different foam types and found mixed results [Lerski, 1999; Mayerhoefer, 2009; Waugh, 2011]. Lerski et al. (1999) found that within single sites of acquisition TA was consistently able to differentiate between foam types. However, this same multivariate function could not be applied successfully to

images acquired at a different site [Lerski, 1999]. Scans for their study were acquired on different hardware, though using the same acquisition parameters [Lerski, 1999]. This indicates that the variability in their results was introduced due to the hardware itself, and that some parametric accommodation needs to be made for different scanners in a multicentre acquisition. Mayerhoefer et al. (2009) studied the effects of both variability in protocol heterogeneity and spatial resolution on TA's discrimination of foam types. They found that texture features extracted from co-occurrence matrices and run-length matrices tended to be more sensitive to variability in scanning parameters than features of other categories [Mayerhoefer, 2009]. However, co-occurrence matrix features were shown to be highly robust to variation in image spatial resolution and were able to perfectly discriminate foam types even at clinical resolutions [Mayerhoefer, 2009]. The third study mentioned, by Waugh et al. (2011), examined the effects of sequence parameters, resolution, and hardware. They analysed a high spatial resolution sequence on a 1.5T scanner, the same sequence on a 3T scanner, and a slightly lower resolution sequence on the 3T scanner which was a faster acquisition [Waugh, 2011]. In contrast to Mayerhoefer et al. (2009), the results of their study indicate that co-occurrence matrix features performed well in foam-type discrimination across all three imaging protocols, and furthermore that these features were effective at discrimination regardless of parameter changes [Waugh, 2011]. Another important finding of this study was that SNR appeared to have no significant effect on classification of foam types, suggesting that TA is robust to noise in an image [Waugh, 2011]. Apart from the scanner itself, other factors such as the coil used may have an impact on the image quality and therefore the computation of TA.

Despite the mixed results of these previous phantom studies, the present analysis indicates that the GLCM features calculated are mostly robust to variation between scanners.

Some differences in the present study which may contribute to different results from previous studies include the present study examining reliability of raw texture values rather than a classification accuracy. Furthermore, this study examines agreement of measurements performed on the same subjects rather than seeking to establish consistency classification. Additionally, the present study examines 3D TA in contrast to the 2D, slice-based TA performed in the others [Lerski, 1999; Mayerhoefer, 2009; Waugh, 2011]. Given that there are slight differences in protocol between Siemens and GE scanners in the present study, these results also suggest that TA is robust to mild variation in scanning parameters. It is unclear why exactly features *corrp* and *cshad* showed reduced reliability compared to the other calculated features. However, trends in reliability for each feature might be explained by the nature of the respective mathematical computations that they represent. Features *corrp* and *cshad* are described as being measures of linear dependency of grey level intensities, and matrix asymmetry and skew, respectively (Table 2). In comparison, *autoc* is described as a measure of repetitive or recurring voxel intensities, meaning that a more homogeneous tissue would carry a higher *autoc* value. It stands to reason then that *corrp* and *cshad* may be more sensitive to slight and single variations in intensity in the calculated matrix involving asymmetry and linear correlation of values and would therefore be more affected by mild variation in scanning conditions. This might account for reduced reproducibility of these features compared to others which examine homogeneity and repetitive recurrence of values.

For features reporting high inter-site reliability, there were several ROIs which had a reduced ICC compared with the others. The most common of these ROIs were the amygdala, the hippocampus, and the thalamus. Scans acquired on different hardware may look different from each other in terms of the relative grey levels in the image. Furthermore, at increased field

strength signal dropout may occur in the more medial portions of the brain. This is typically not a substantial issue in studies using 3T scanners, though it can contribute to a lack of image contrast. Tissue segmentation also seems to be somewhat inconsistent in its success for the differentiation of brain structures [Helms, 2009; Wonderlick, 2009; Pereira, 2010]. Helms et al. (2009) suggest that T1 images are often unable to provide enough tissue contrast in deep brain structures to accurately and reliably perform automated segmentation of them. Wonderlick et al. (2009) describe their results in which some subcortical structures such as the caudate and the thalamus appeared to have more consistent and accurate segmentation than other subcortical structures. They suggest that improved performance on certain structures is likely due to the presence of WM and CSF adjacent to them, allowing more accurate differentiation by the segmentation algorithm [Wonderlick, 2009]. This holds true in part for the present study. The caudate ROI did have high ICC values across the board, both for intra-site and inter-site measurements. However, the thalamus saw some reduced reliability in the inter-site comparisons suggesting that tissue contrast was inconsistent between scanning hardware. This variation in tissue contrast may have contributed to reduced ICCs in other structures as well.

All images were aligned automatically to ACPC orientation prior to texture feature calculation. This is done because texture is calculated in the image native space using a GLCM in set and standard orientation. This means that if images are misaligned in their native space, texture might be calculating different relative values based on the offset of the image in question. Upon visual comparison the automatic realignment does look very consistent, but of course there is the possibility of very slight variations between scans. This is a potential source of variance in the texture values calculated from scan to scan.

Apart from the steps already taken to ensure reliable results such as a harmonised protocol, some future steps could be included to mitigate any remaining variability. One such course of action might be a standardisation of texture values across sites. If there is a slight shift of values reported between each site of acquisition, it might be beneficial to scale these values such that each site is fully comparable. A possible way of doing this might be to calculate z-scores for voxel-wise texture values, thus making values comparable based on variation from the mean rather than a raw value. Another possible way to minimize variation is to standardise brightness and contrast histograms prior to texture feature calculation such that relative voxel intensities would be consistent prior to feature extraction. Additionally, the inclusion of more subjects for this type of analysis may increase the statistical power. Further to this, it may be useful to include several ALS patients in this type of analysis, as that may be a better measure of whether TA is truly reliable and fit for analysis is the context of patients. However, this may prove to be logistically challenging depending on level of impairment. Another challenge with including ALS patients is that scans at each site would need to be done as close together as possible temporally so as to avoid introduction of any variation caused by the progression of the disease.

The results of the study, however, do indicate that this method of 3D, voxel-wise texture analysis is relatively consistent and reliable both within and between sites. This supports its implementation for the study of cerebral degeneration in a patient population, as we can say with confidence that detected changes are due primarily to the disease course rather than random error of the software.

5.5. Conclusion

In summary, the results of this experiment indicate that TA is reliable both within and between sites of image acquisition. Some features performed better than others, and they should therefore be focused on for future studies. Reliability was reduced in some structures, though this may be due to reduced tissue contrast in those regions of the brain. As expected, reliability was reduced when compared between sites, though these reductions were not substantial enough to suggest that TA cannot be used on data acquired from multiple centres. Overall, the experiment supports further implementation in multicentre studies of cerebral degeneration.

6. Experiment 2: A Multicentre Study of ALS Pathology

6.1. Introduction

The second experiment of the present study aims to implement TA as a means to study cerebral degeneration in ALS patients. The data for this study was also acquired using a harmonised protocol from multiple centres across Canada. Multicentre imaging studies are important as they can contribute to larger samples in diseases which are less common. Furthermore, as mentioned in the previous chapter, a multicentre study examining disease pathology can provide support for future implementation in clinical settings. TA has been implemented in previous studies of disease pathology including Alzheimer's disease, MS, epilepsy, and ALS [Bonhila, 2003; Antel, 2003; Sikio, 2015; Oppedal, 2015; Sørensen, 2016; de Albuquerque, 2016; Maani, 2016]. Previous studies have demonstrated success in differentiation between patients and controls – or even between phenotypes of pathology – with high sensitivity and specificity. The goal of the present study is to examine cerebral degeneration in ALS patients on a multicentre scale, and further to test whether texture abnormalities detected correlate with disease severity as measured in clinic. Additionally, the present study looks to examine how the spatial distribution of texture abnormalities compares between sites.

6.2. Materials and Methods

6.2.1. Study Participants

Participants for Experiment 2 were recruited as a part of the Canadian ALS Neuroimaging Consortium (CALSNIC), a multicentre effort to evaluate potential neuroimaging biomarkers in ALS. CALSNIC is ongoing with the goal of providing standardized clinical and MRI evaluations for patients with ALS at centres across Canada. All data for the study was collected prospectively

with a harmonized clinical and imaging protocol. Patients were included in this study only with a diagnosis of ALS based on El Escorial criteria. Subjects were excluded if they had prior history of other neurological or psychiatric disorders, or significant head injury. Additionally, subjects with claustrophobia, or pacemakers and other foreign metallic bodies are ineligible for participation in MRI studies. Participants for the present study were recruited at four sites across Canada: Edmonton – Peter S. Allen MR Research Centre (patients, n = 20; controls, n = 20), Calgary – Seaman Family MR Research Centre (patients, n = 10; controls, n = 10), Montreal – Montreal Neurological Institute and Hospital (patients, n = 13; controls, n = 7), and Toronto – Sunnybrook Research Institute (patients, n = 21; controls, n = 11). Samples were age and gender matched to the best of our ability despite constraints of in-clinic recruitment. A neurological examination was performed on each ALS patient at their study visit. A scale of UMN burden was derived from data collected during these neurological evaluations. It consisted of two lateralized subscores for the right and left sides of the body, and a subscore for jaw-related symptoms. Each of the left and right subscores accounted for increase in tone and reflex for the respective arms and legs, as well as the presence of Babinski's sign or clonus in the lower extremity. The final subscore accounted for a brisk reflex or clonus in the jaw. Presence of each of these listed signs added a value of 1 to the total score which was measured out of 14. Finger and foot tapping were also measured for each patient and healthy control during study visits. Finger tapping was measured by having the participant place their hand on a surface and tap their finger as many times as they could in 10 seconds. Foot tapping was similarly performed by having the participants plant their heel and tap their foot as many times as they could in 10 seconds. These tapping scores are measures of UMN function. ALSFRS-R is a questionnaire that assesses disease severity with a score of 0-48 in which

a lower score indicates greater disease-related impairment. Participant demographics are summarized in Table 5.

Table 5. Summarized participant demographic information. Values noted for age, symptom duration, ALSFRS-R, forced vital capacity (FVC), and UMN score are medians with the associated range of values in the sample in brackets.

		Patients (n = 64)	Controls (n = 48)
Age (years)		57 (33-86)	55.5 (29-69)
Site of Onset	Bulbar	11	-
	Limb	50	-
	Respiratory	3	-
Symptom Duration (months)		25.5 (8-130)	-
ALSFRS-R Score		40 (22-47)	-
FVC (%)		3.32 (1.95-6.79)	-
UMN Score		5 (0-11)	-

6.2.2. MRI Acquisition Protocol

3D T1 scans were acquired at all four sites on clinical research MRI systems operating at 3 T: Siemens Prisma (Erlangen, Germany) in Edmonton, Siemens Trio (Erlangen, Germany) in Montreal, and General Electric MR750 (Milwaukee, WI) in Calgary and Toronto. Scan acquisition was performed with the same protocol as was detailed in the Travelling Heads experiment, though only four of the five sites were included. Scans were acquired with an MPRAGE sequence on Siemens scanners (TR = 2300 ms, TE = 3.43 ms, TI = 900 ms, flip angle = 9°, FOV = 256 × 256 mm, resolution = 1 mm × 1 mm × 1 mm), and using FSPGR on GE scanners (TR = 7400 ms, TE = 3.1 ms, TI = 400 ms, flip angle = 11°, FOV = 256 × 256 mm, resolution = 1 mm × 1 mm × 1 mm).

6.2.3. Data Preprocessing

Data were converted from raw DICOM format to Niftii files using dcm2nii converter (MRIcron). These files were then realigned manually to ACPC orientation using Mango software. From here, the data was modulated, segmented into grey and white matter, and bias corrected using the high dimensional DARTEL algorithm in the VBM8 toolbox of SPM8 (http://www.fil.ion.ucl.ac.uk/spm/). During this step, a deformation field was also created for subsequent normalization of texture maps into MNI standard space.

6.2.4. 3D Texture Analysis

3D texture analysis was performed and calculated exactly as described in Experiment 1. Furthermore, the same features were calculated for this analysis as were in Experiment 1.

6.2.5. Pooled Voxel-Wise Statistical Analysis

Cross-sectional analysis of the pooled samples was performed using a full factorial model in SPM8. Factors in this analysis were diagnosis and site with age as an additional covariate. Furthermore, the analysis was run both with and without controlling for brain parenchymal fraction (BPF – a measure of global brain atrophy). This model was used to examine both the main effect of diagnosis on calculated texture feature values, and any interaction between site of acquisition and the diagnosis of the subjects. Significant results were accepted at a p-value of <0.001 and a voxel cluster threshold of 50. Clusters are groups of voxels deemed to be significantly different between groups. Single voxels or very small clusters which are significant are often attributable to false positive error. Thus, only groups of significant voxels exceeding a threshold size are deemed to be truly pathological in nature, and all other groups are eliminated. No multiple comparisons corrections were performed due to the exploratory nature of this study.

Further to this analysis, the model examined the interaction between site and diagnosis. Significant results were accepted at the same threshold as previously described.

6.2.6. Site-Specific Voxel-Wise Statistical Analysis

Cross-sectional analysis of each site's respective samples individually was performed using 2-sample t-tests, again in SPM8. Within these comparisons, subject age was assigned as a covariate of the analysis. These results were also accepted at $p<0.001$ and a voxel cluster threshold of 50. Differences between sites for demographics were compared using one-way ANOVA. Parametric testing was performed due to the potential of differences in sample spread and distribution. Subject information broken down by site is included in Table 6.

Table 6. Patient and control demographic information by site listed as medians with ranges in brackets. * indicates a significant difference between sites. ALSFRS-R was significantly different at $p<0.001$, and symptom duration (SD) was significant at $p<0.002$.

		Calgary		Edmonton		Montreal		Toronto	
		P (n=10)	C (n=10)	P (n=20)	C (n=20)	P (n=13)	C (n=7)	P (n=21)	C (n=11)
Onset	Limb	n=8	-	n=16	-	n=9	-	n=20	-
	Bulbar	n=2	-	n=4	-	n=4	-	n=1	-
Age (years)		60 (41-82)	55 (40-69)	58.5 (37-74)	60 (37-68)	57 (41-86)	54 (38-66)	54 (33-88)	49 (29-68)
ALSFRS-R*		33 (22-45)	-	41.5 (32-47)	-	40.5 (33-44)	-	38 (28-47)	-
SD (months)*		46.5 (21-117)	-	19 (11-60)	-	18 (8-72)	-	39 (8-130)	-
FVC (%)		3.02 (1.95-4.61)	-	2.49 (2.41-4.88)	-	3.76 (2.67-4.98)	-	3.32 (1.98-6.79)	-
UMN score		4.5 (2-9)	-	5 (1-11)	-	5 (2-8)	-	5 (0-11)	-

6.2.7. ROI-Based Correlations

For the ROI analysis clinical measures were to be correlated with areas of significant difference in the motor regions of the brain as detected by the full factorial model. Based on the full factorial model's results for the main effect of diagnosis, a mask of significant texture abnormalities in the internal capsule as detected by feature *autoc* was extracted using xjView toolbox (http://www.alivelearn.net/xjview). This structure was extracted in unilateral and bilateral masks. As mentioned previously in the Preliminary Analyses section, this structure was

chosen based on the idea that the detected abnormalities in the internal capsule might represent focal pathology of the disease process and potentially demonstrate a less diluted link between cerebral degeneration and the outward signs of UMN impairment. The comparisons were made using partial correlations which controlled for both age and site in the analysis. Due to the nature of the partial correlation setup in MedCalc, site was controlled for using dummy variables. The results were accepted as being significant at $p<0.05$.

6.2.8. ROC Analysis

ROC analysis was performed by using a logistic regression model to produce predictive values, which were then used as the classification parameters in the ROC. The logistic regression was used in this way such that it was possible to control for age and site in the analysis. The *autoc* values from the bilateral internal capsule ROI were used for this classification. Once the predictive values for this analysis were saved, they were input and allowed classification based on a threshold defined by the statistical model for differentiation based on diagnosis. Area under the curve (AUC), sensitivity, and specificity were examined. Results were again accepted as being significant at $p<0.05$.

6.3. Results

6.3.1. Pooled Voxel-Wise Analysis

The results of this portion of the study indicate that different texture features detect different changes in the brain. Results which were not corrected for BPF showed more diffuse abnormalities. Five of the seven features showed significant differences between patients and controls at $p<0.001$. For feature *autoc* texture differences were detected in the internal capsule, but also in the frontal and temporal lobes. Features *contr* and *cprom* showed abnormalities in the

anterior cingulate cortex. *Energ* detected patient control differences in the internal capsule as well as in the cerebellum and the frontal lobe. *Indnc* detected significant differences in the temporal lobe white matter. These results are seen in Figure 14, and significant clusters are summarised in Table 7.

It should be noted that any clusters appearing outside the brain area in Figure 14 and Figure 15 are, in fact, within the brain. It appears this way due to the limited space of the glass brain format. However, when overlaid on a T1-weighted image, all significant clusters rest within the brain.

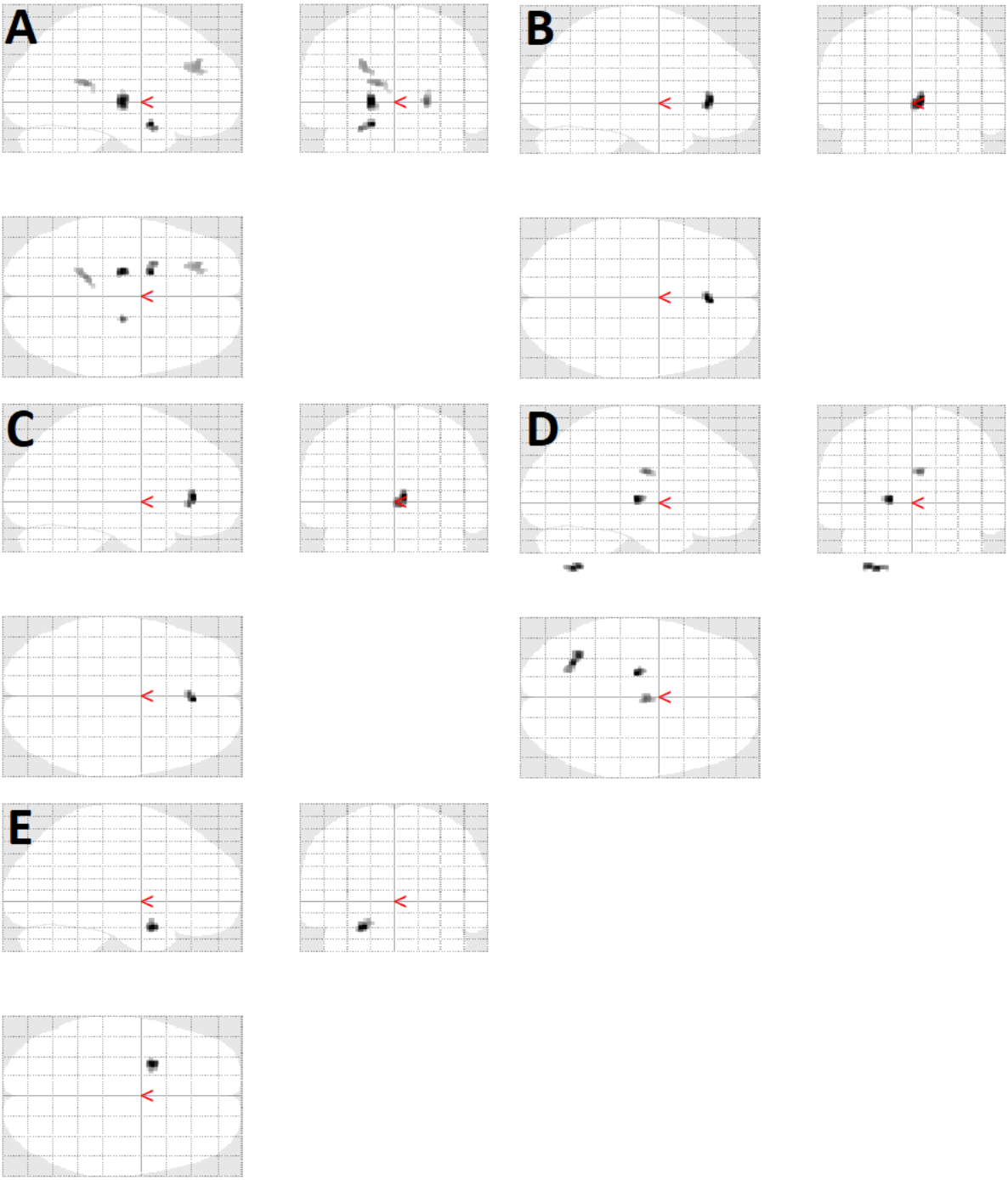

Figure 14. Glass brain representations of features showing significant differences between ALS patients and controls without correction for BPF. A) *autoc*. B) *contr*. C) *cprom*. D) *energ*. E) *indnc*.

Table 7. Summary of significant voxel clusters in pooled analysis not correcting for BPF. MNI coordinates are listed in columns X, Y, and Z.

Feature	Structure	Cluster Size	F-stat	p-value	X	Y	Z
	L internal capsule	135	29.64	<0.001	-20	-16	-2
	L entorhinal cortex	72	28.44	<0.001	-18	5	-20
autoc	R internal capsule	55	22.58	<0.001	21	-16	-2
	L splenium	56	18.93	<0.001	-14	-42	13
	L middle frontal gyrus	82	17.38	<0.001	-24	38	28
cprom	Anterior cingulate cortex	107	28.41	<0.001	5	35	1
cprom	Anterior cingulate cortex	104	31.35	<0.001	5	35	3
	L internal capsule	55	24.81	<0.001	-18	-18	1
energ	Cerebellum	106	23.17	<0.001	-27	-64	-57
	Corpus callosum	59	18.72	<0.001	3	-12	25
indnc	L entorhinal cortex	92	22.44	<0.001	-24	6	-23

For the analysis which controlled for BPF, four of the seven calculated texture features detected significant results between ALS patients and controls at $p<0.001$. These abnormalities were typically more focal than the previous analysis. Specifically, for features *autoc and energ* significant texture abnormalities were present in the internal capsule of the CST. Furthermore, for features *contr* and *cprom* significant abnormalities were detected in the anterior cingulate cortex. Additionally, these results were supplemented by an interaction statistic examining the effect of site on diagnosis. Most features were largely unaffected, with *autoc* showing no interaction at all. Results can be seen below in Figure 15, and significant clusters are summarised in Table 8.

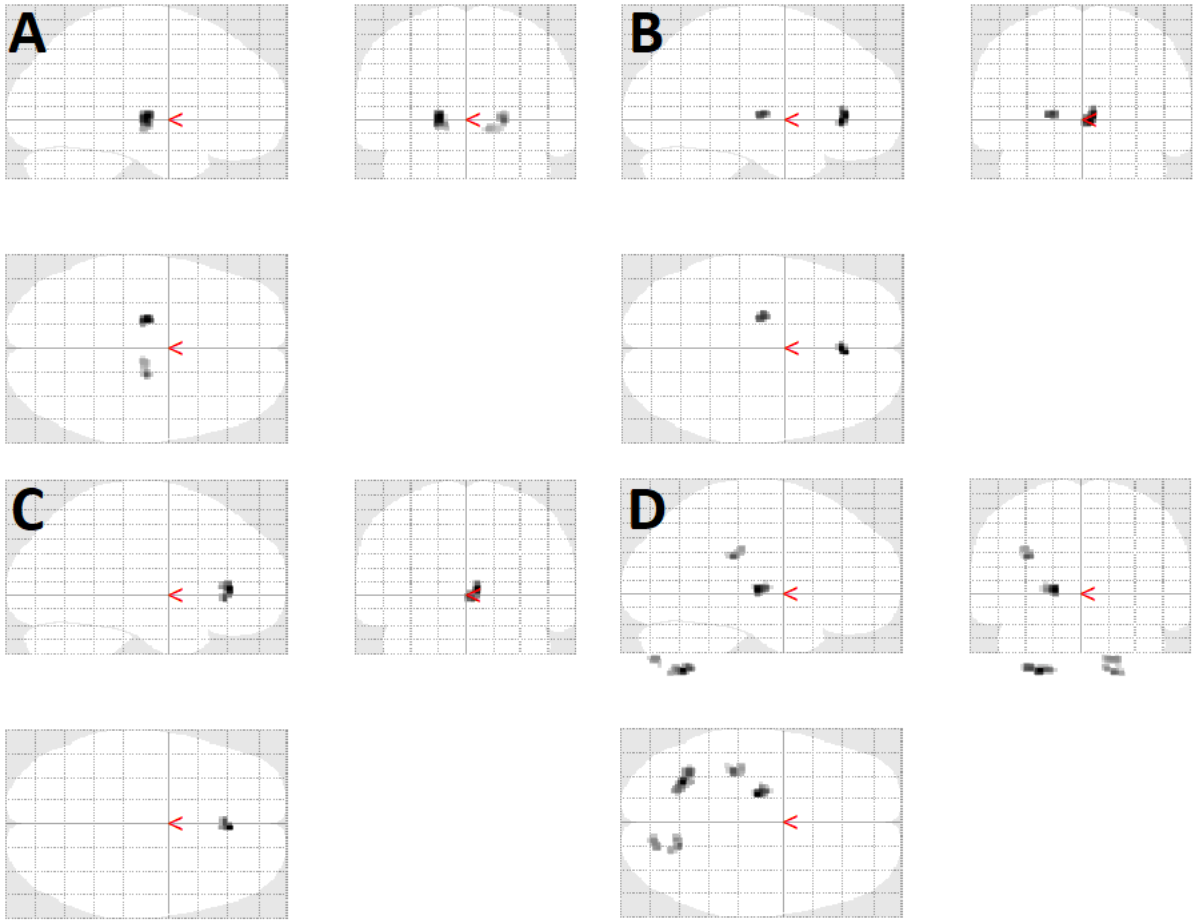

Figure 15. Texture features demonstrating significant differences between ALS patients and controls when corrected for BPF. A) *autoc*. B) *contr*. C) *cprom*. D) *energ*.

Table 8. Summary of significant voxel clusters for pooled analysis corrected for BPF. MNI coordinates are listed in columns X, Y, and Z.

Feature	Structure	Cluster Size	F-stat	p-value	X	Y	Z
autoc	L internal capsule	139	28.76	<0.001	-18	-16	0
	R internal capsule	90	21.67	<0.001	21	-16	-2
contr	Anterior cingulate cortex	85	24.07	<0.001	2	32	-3
	L internal capsule	57	20.63	<0.001	-20	-16	3
cprom	Anterior cingulate cortex	94	27.14	<0.001	5	35	3
energ	L internal capsule	108	28.41	<0.001	-18	-18	1
	L inferior parietal lobule	158	27.91	<0.001	-27	-64	-57
	Cerebellum	65	21.77	<0.001	-35	-33	25
	Cerebellum	56	20.42	<0.001	18	-66	-59
	Cerebellum	58	18.07	<0.001	17	-81	-48

6.3.2. Site-Specific Voxel-Wise Analysis

Significant texture abnormalities were detected for most features at each individual site. However, these patient-control differences were not consistent across sites of acquisition. The most consistent feature in this site-specific analysis was *autoc*, showing change in regions including the CST and throughout the frontotemporal regions. Other features demonstrated significant differences in the cerebellum, the thalamus, and the cingulate cortex as well as multiple regions in the frontal and temporal lobes. These changes were also not entirely in pathologically relevant or expected regions with some changes occurring in areas including the occipital lobe. Results for *autoc* are shown in Figure 16.

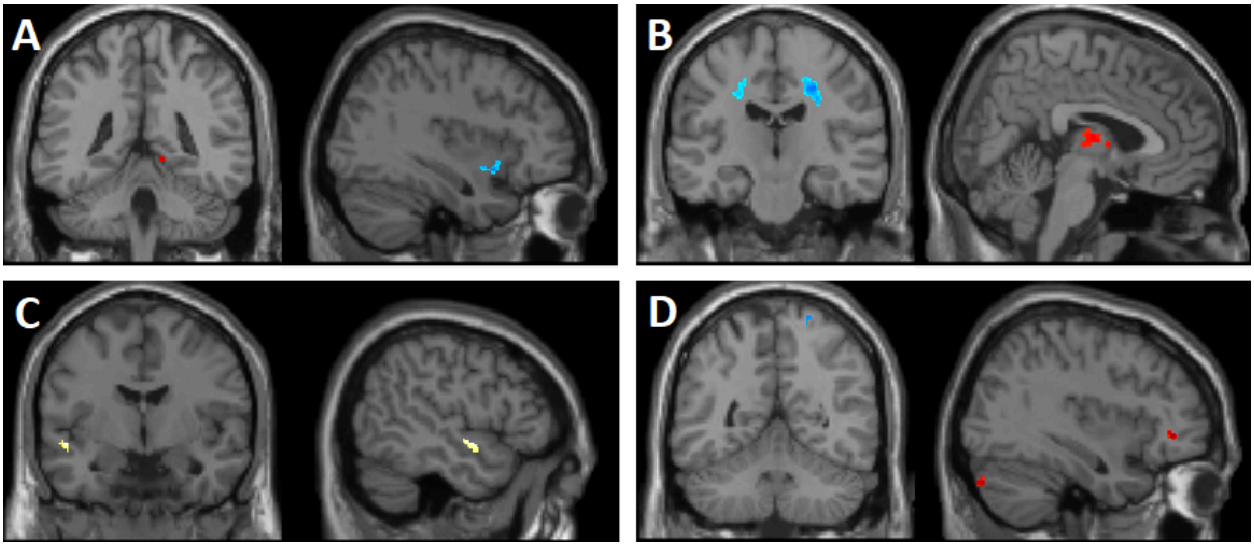

Figure 16. Cross-sectional analysis of feature *autoc* for each individual site. In panels A), B), and D) blue indicates an increase in *autoc* for patients compared to controls, and red indicates decreased *autoc*. In the Montreal sample (C) only a significant decrease was detected and is indicated in yellow. A) Significant texture abnormalities in the Calgary sample occurred in several areas of the brain including Brodmann area 30, Brodmann area 13, and the anterior cingulate cortex. B) Significant differences in the Edmonton sample included the corona radiata of the CST, the thalamus, and several regions in the temporal lobes. C) The Montreal sample showed significant texture abnormalities only in the left superior temporal gyrus. D) Significant texture differences occurred in Toronto ALS patients in the cerebellum, the middle frontal gyrus, and the superior parietal lobule.

6.3.3. ROI-Based Correlations

The results of the correlation analysis showed that there was a significant correlation between feature *autoc* values in the internal capsule and the score of UMN burden. Additionally, three features correlated with BPF. Within this ROI there were no significant correlations between texture values and finger and foot tapping scores, nor were there any correlations between texture and ALSFRS-R scores. Significant results are summarised in Table 9.

Table 9. Summary of significant correlations between clinical measures and texture values in the internal capsule. Both UMN score and BPF were compared with a bilateral ROI of the internal capsule.

Correlate	Feature	ROI	n	p-value	Correlation coefficient (r)
UMN total score	*autoc*	Internal capsule	60	0.0091	0.345
BPF	*contr*	Internal capsule	64	0.0146	0.314
	energ	Internal capsule	64	0.0089	-0.335
	indnc	Internal capsule	64	0.0085	-0.337

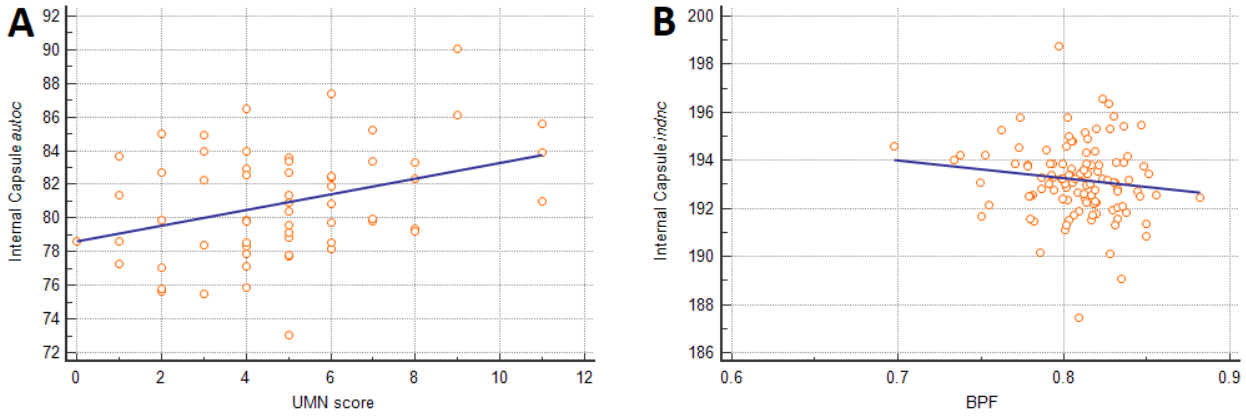

Figure 17. Scatterplots for the significant correlation of A) *autoc* values in the internal capsule with UMN scores, and B) *indnc* values in the internal capsule and BPF. Information for each of these correlations is listed in Table 9.

6.3.4. ROC Analysis

The results of the ROC analysis showed that all of the features examined were able to significantly differentiate between patients and controls once corrected for age and site. All features differentiated at $p<0.0001$. These results are summarised in Table 10 and Figure 18.

Table 10. Significant results in ROC analysis.

Feature	ROI	Subjects (n)	AUC	p-value	Sensitivity	Specificity
autoc	Internal capsule	112	0.840	<0.0001	78.12	79.17
contr	Internal capsule	112	0.772	<0.0001	71.87	77.08
corrp	Internal capsule	112	0.719	<0.0001	62.50	79.17
cprom	Internal capsule	112	0.720	<0.0001	65.62	79.17
cshad	Internal capsule	112	0.726	<0.0001	68.75	72.92
energ	Internal capsule	112	0.800	<0.0001	57.81	91.67
indnc	Internal capsule	112	0.789	<0.0001	75.00	75.00

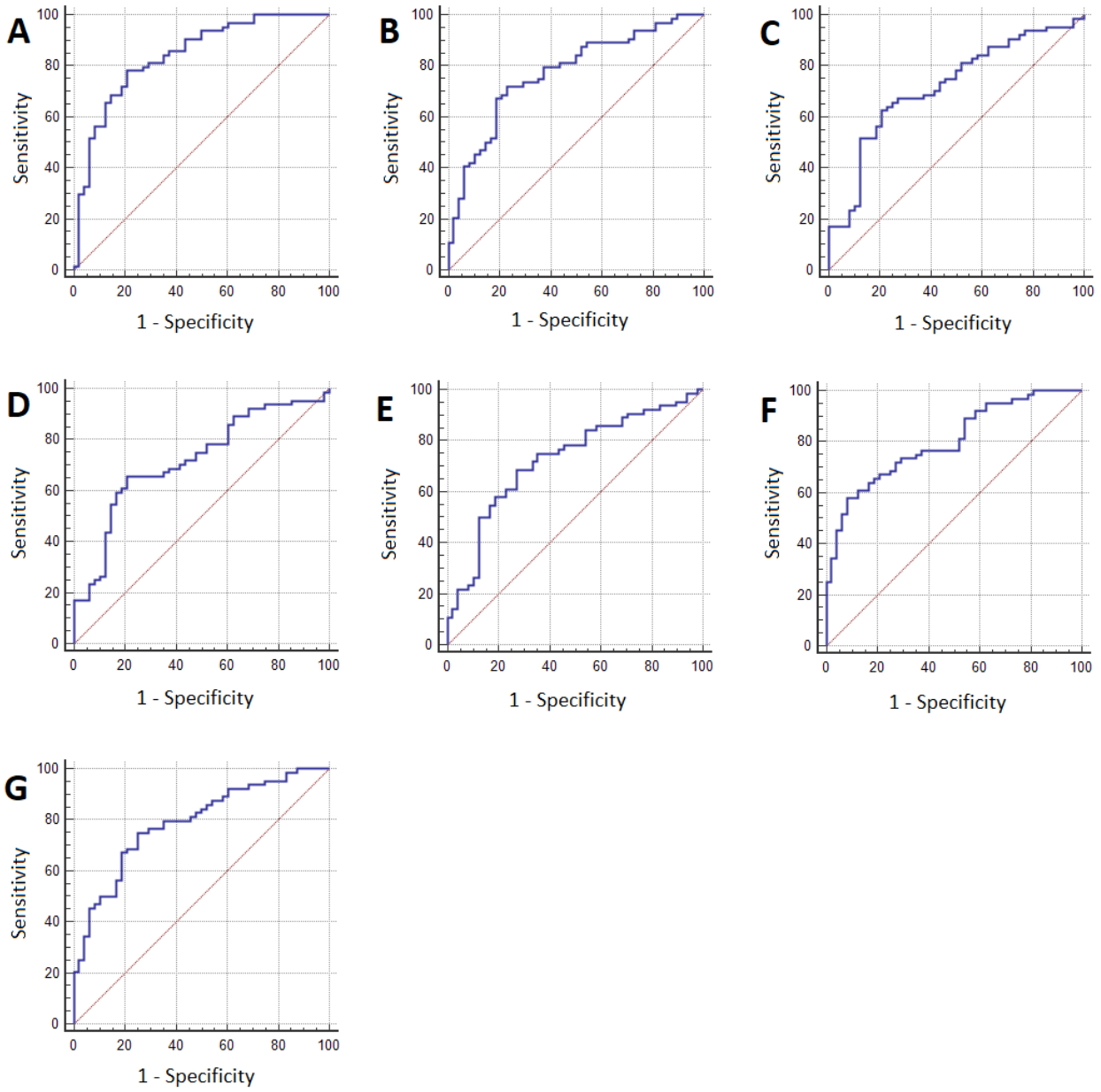

Figure 18. ROC curves for all calculated texture features. All results were significant at p<0.0001. A) Feature *autoc*. B) Feature *contr*. C) Feature *corrp*. D) Feature *cprom*. E) Feature *cshad*. F) Feature *energ*. G) Feature *indnc*. Results are summarised in Table 10.

6.4. Discussion

The results of the pooled voxel-wise analysis are exciting in that they do, in fact, detect texture abnormalities in pathologically relevant areas of the brain. The results for features *autoc* and *energ* were particularly interesting in that they detected slightly different areas of involvement when controlling for BPF compared to when not controlling for it. The significance in this, it could be argued, is that texture is able to detect different types of pathological change in the brain. When carrying out an analysis which does not account for BPF, the changes detected can be partially attributed to atrophic change in the brain. However, when BPF is used as a covariate, it was thought that pathological changes that are primarily atrophic in nature would be controlled for and eliminated from the results. What is left are texture abnormalities in ALS patients which are not entirely atrophic in nature and can be attributed – at least in part – to some other form of pathology. It is possible though that these differences between the two analyses could be attributable to some other confounding factor. Furthermore, texture changes which disappear when controlling for BPF may correlate with but still be unrelated to global atrophy. Even so, texture may be detecting different forms of pathological change in the brain. Due to the fact that texture is a measure of voxel intensity patterns, detected texture change could be due to any number of mechanisms which would slightly alter the relative intensities of the imaged tissue. As was discussed in the sections surrounding pathogenesis and pathology, there are several potential processes in ALS which could be contributing to texture changes. Apart from a general loss of neuronal and glial cells, some possibilities are the presence of intracellular and cytoplasmic inclusions such as C9orf72, FUS, TDP-43, and SOD1 aggregations. Additionally, other pathological changes such as vacuolisation, or spongiosis of neuronal and surrounding cells, and reactive astrogliosis in areas of neuronal loss could be responsible [Saberi,

2015; van Es, 2017; Chio, 2014]. With no correction for BPF, *autoc* detects texture abnormalities in the internal capsule, the corpus callosum, the middle frontal gyrus and Brodmann Area 28. However, when corrected for BPF, *autoc* showed that significant patient control differences remained in the internal capsule region of the CST. The internal capsule is frequently reported as an area of ALS pathology [Schuster, 2016; Sarica, 2017; Masuda, 2016; Chapman, 2014]. These studies reporting pathology in the internal capsule are primarily diffusion imaging studies examining changes in measures of FA and RD along the CST [Schuster, 2016; Sarica, 2017; Masuda, 2016; Chapman, 2014]. Changes in FA and RD are largely representative of microstructural change. Changes in RD are seen as representative of reduced myelin or a change in myelin health, whereas FA can be representative of both myelin and axonal degeneration [Alexander, 2007; Chapman, 2014]. Given that changes in diffusion metrics are representative of microstructure rather than gross atrophy, this supports the claim that texture is able to examine various forms of pathology in vivo. In addition to changes in diffusion metrics, Sugiyama et al. (2013) note that tissue samples from the internal capsule show astrogliosis, accumulation of macrophages, and an abnormal pallor to the myelin. Some of the other detected abnormalities by *autoc* including the cluster in the middle frontal gyrus are known pathology in ALS. In fact, the middle frontal gyrus is recognised as an area of both atrophy and TDP-43 pathology [Brettschneider, 2012; Brettschneider, 2013]. This co-occurrence of both atrophic and protein pathology supports the idea that significant clusters disappearing when controlling for BPF may be attributable to multiple pathologies. Feature *energ* showed similar results in which case there were texture abnormalities present in the left internal capsule, corpus callosum, and the cerebellum without BPF correction, but the corpus callosum differences disappeared when corrected for BPF. Other features such as *contr* and *cprom* detected only changes which were

present in both corrected and uncorrected analyses. These significant differences occurred in the internal capsule and the anterior cingulate cortex. While it has been found that the anterior cingulate cortex can be a region of GM volume reduction in ALS, studies have also found changes in diffusion metrics and TDP-43 inclusions [Menke, 2018; Tan, 2017]. These studies provide further support for TA's ability to detect various pathological processes. This is of importance as these particular areas could be points of interest in future studies looking to examine points of major pathology in ALS patients. Only one feature that detected texture abnormalities without BPF correction did not detect changes when it was corrected. This feature was *indnc*, which showed only significant differences in Brodmann Area 28 (entorhinal cortex) – similar to those detected by an uncorrected *autoc*. This feature lends further support to the changes detected in this particular brain region. It also suggests that this instance of texture change in patients may be atrophic or more overt in nature, rather than a microscopic change such as inclusions. Takeda et al. (2007) explain that degeneration of the entorhinal cortex in ALS patients has been well observed. This degeneration is particularly common in ALS patients with FTLD or dementia, and it can also involve the presence of ubiquitin-positive inclusions [Takeda, 2007]. It is also worth note that the two features in the current analysis which showed no significant differences between ALS patients and healthy controls were demonstrated to have poor reproducibility between sites of acquisition (Experiment 1). This may be a contributing factor to their inability to detect cerebral degeneration, especially given the heterogeneous nature of the disease in question.

While these results do suggest a detection of pathology, future studies should look to expand on this in a multimodal analysis of the types of pathology present. It will be important to establish a more concrete meaning behind what exactly these texture value changes represent *in*

vivo. One potential for analysis of specific pathology would be using DTI in order to examine WM microstructural changes in conjunction with texture changes. Another potential option for this type of study would be to use PET imaging as a comparison for disease severity and pathology present. Techniques such as FDG-PET have been used as a measure of glucose metabolism in ALS, and by extension a measure of neuronal health. Furthermore, *ex vivo* analyses of subject brain tissue with H&E and LFB stains might provide insight to the presence of different pathological processes linked to changes detected by each texture feature. This could be elaborated upon by studying texture abnormalities longitudinally in which the expected observation would be a linear change in texture values as time progresses. In fact, the framework for CALSNIC includes a longitudinal collection of data which carries through to post-mortem, should the patients consent to this portion of the study. Future implementation of post-mortem scans and sections will help to establish a link between the neuroimaging analysis and the pathology present in our study sample. This is of particular importance in that pathological heterogeneity for ALS patients does not just mean between patients, but also that individuals might have different types of pathology which affect different areas of the brain. An example might be that the disease could develop in a patient as a degeneration of axonal and myelin cells in the CST, but only present with TDP-43 inclusions in the anterior cingulate cortex. Nonetheless, TA detects some differences in the pathologies present in the brain based on the feature in question. Therefore, a multimodal analysis involving TA would be a novel method of examining pathology in ALS.

The analysis of individual sites adds another layer to the study in that it provides an examination of the heterogeneity between sites. It was hypothesised at the beginning of the study that each site of acquisition would present with similar areas of texture abnormalities. This was

to represent both similar pathology between samples and TA's robustness against using different scanners for image acquisition. The results of the study showed that this hypothesis was not the reality of the situation. However, based on several factors of the analysis it might be suggested that these differences in texture are due to the composition of the samples rather than the technique itself. Firstly, the acquisition protocol for CALSNIC is harmonised. The protocol was developed with target spatial parameters for scans to be identical in addition to image quality with regard to SNR and CNR. Acquisition parameters were adjusted slightly based on the make and model of the machines to accommodate their specific limitations and ensure a similarity of the images. However, previous literature has demonstrated that differences in scanner hardware can be in part responsible for variation [Takao, 2013; Kruggel, 2010]. A VBM-based study by Takao et al. (2013) showed that even using two scanners of the exact same model for a "longitudinal" study of healthy controls can yield a significant longitudinal "change" in the brain which is more severe than atrophic changes seen in Alzheimer's disease. This was in comparison to subjects scanned longitudinally on the same scanner who demonstrated little to no significant changes between scans. In addition to this, scanner software upgrades were a major source of inconsistency for scan-rescan reliability [Takao, 2013]. The data acquired for the CALSNIC study was tested for reliability and reproducibility both within and between sites of acquisition. The results of this study indicated that five of the seven texture features used in the analysis were highly reliable and reproducible both within and between sites (Experiment 1). In addition to the protocol itself, an effort was made to ensure no software upgrades were done in the duration of the present study. With the careful collection of harmonised data, effects of hardware and software on the scans have been mitigated as much as possible. A potential source of inconsistency between sites in the cross-sectional analysis is the small size of each sample. This

is for a couple of reasons. Firstly, with small samples it is more difficult to derive a representative statistical sign of pathology without seeing noise which would typically be washed away with more subjects. Another reason is the heterogeneity of ALS pathology itself which exacerbates the statistical model's issues. With ALS presenting with such diversity between individuals, there is a high chance that this variability would come through in group comparisons using different samples. This is supported by a significant difference in ALSFRS-R scores and symptom duration between sites despite no significant difference in patient ages. Patients from Edmonton and Montreal had higher ALSFRS-R scores and a shorter symptom duration, indicating that these patients generally have less advanced pathology than the other two sites. This is not represented in any obvious way in the voxel-wise results, but it is something that should be investigated in future analyses. With each site having different samples and sample sizes, it is reasonable to expect that each site would detect different texture abnormalities. For these reasons, it seems reasonable to assume that this variability is not something to attribute to TA itself. In fact, the pooled full factorial model demonstrated that there was little effect caused by interaction between site and diagnosis. This effect was particularly minimal for some features such as *autoc* which demonstrated no interaction at all. This is in line with *autoc* being rather consistent compared to some of the other features examined in the individual-sites analysis. Despite this variability, some of the texture abnormalities occurred in pathologically relevant areas of the brain including the precentral gyrus and the CST. Furthermore, some areas of change occurred in less frequently cited areas of ALS pathology such as the cerebellum and the thalamus [Kim, 2016; de Albuquerque, 2016]. It is important to be cautious of these significant clusters given that some clusters appear in areas of the brain which are not relevant to the pathology. However, it is promising to see some more subtle changes which have been previously detected

in ALS-related literature [de Albuquerque, 2016; Lillo, 2012; Masuda, 2016; Kim, 2016; Kim, 2017].

Correlations between significant abnormalities in texture values and clinical measures of disease severity are another metric which is important for the validation of TA. Total UMN score did correlate significantly with *autoc* in the internal capsule. The significant correlation here is important as this aligns variation in TA values and the degeneration of UMN through clinical signs. It provides evidence that TA is acting as an objective measure of UMN degeneration. This is exciting because in clinic there are no truly objective measures of UMN disease burden. As is measured by the UMN burden scale that was created for this study, neurologists would typically look for the presence or absence of symptoms such as hyperreflexia and spasticity. However, with texture values being tied significantly to this type of pathology it is promising that there may be less reliance on the subjective measures in this complicated diagnostic process. Other clinical measures tested did not correlate. Finger and foot tapping scores were expected to correlate since they are also taken to be representative of UMN burden. However, tapping scores can be complicated by differences in counting between people administering. Of course, there is a hope of consistency based on a standard method of administration, but this is not always the case. Variation is particularly prominent in the case of finger tapping, as it is done more quickly and is therefore more difficult to count accurately. One possible solution for this inconsistency would be the use of counting apps. These apps can count the number of taps on a screen in a certain allotted time and would eliminate any variability between individuals counting taps. I would suggest that this method of administration be standard in future studies. However, tapping scores are further confounded by the presence of LMN degeneration in patients. While tapping is primarily measuring disease burden by UMN degeneration, weakness and atrophy of muscles

due to LMN pathology can significantly reduce one's ability to tap either fingers or feet. This is further complicated by decisions of who we should or shouldn't exclude for this measure. Since ALS is a disease of both types of pathology, it might be argued that all patients should be included regardless of their LMN involvement. It is difficult to exclude based on reduced scores as there is no specific threshold at which a line can be drawn for those whose scores are primarily being affected by UMN or LMN degeneration. Another clinical measure that did not correlate with texture values was ALSFRS-R scores. While there is a hope that all clinical measures of disease severity correlate with TA, it is not altogether surprising that the functional rating scale did not. This is because the scale is more so a measure of LMN degeneration than it is for UMN burden. Most of the questions in the ALSFRS-R examine patients' ongoing ability to perform activities of daily living – some examples being writing, climbing stairs, walking, and dressing. While these activities may be affected to some degree by UMN dysfunction, they are primarily hindered by muscle atrophy caused by LMN involvement. In contrast, TA performed in the brain is taken to be primarily a measure of UMN involvement, so it is reasonable to expect that there is not a complete overlap or correlation between the two measures. ALS disease involvement is complicated, and we know that patients experience variable levels of UMN and LMN pathology depending on the individual in question. For that reason, a lack of correlation here is disappointing but not shocking or alarming.

A final correlation that was performed was that between texture values and BPF. As described previously, BPF is a measure of global brain atrophy. The objective motivating this experiment was to examine whether a region of focal degeneration in the brain might be representative of the amount of atrophy throughout the entire brain. If so, this focal region might represent an area of initial pathology, the severity of which could be associated with the amount

of global change seen in that individual. Interestingly, BPF did correlate significantly with texture values for three different features in the internal capsule. This further supports the internal capsule being a major area of interest in ALS pathology. Based on the present study, as well as previous ALS literature demonstrating internal capsule degeneration [Schuster, 2016; Sarica, 2017; Masuda, 2016; Chapman, 2014], it might be suggested that the internal capsule be a point of focus in future studies for the detection of diseases on the ALS spectrum. The internal capsule in this case, as shown by *autoc* and *energ* might not represent entirely atrophic change itself but may represent a point of origin which is integral to the process of atrophy in ALS. Two main hypotheses for the spreading pattern of ALS pathology are the dying-forward hypothesis and the dying-back hypothesis [Korner, 2011; Iyer, 2018]. The dying-forward hypothesis suggests that ALS pathology originates in the motor neurons of the central nervous system, and the dying-back hypothesis suggests that pathology starts at the neuromuscular junction [Iyer, 2018]. However, it may be the case that neither of these are true per se. ALS symptom onset is typically focal and spreads to other areas of the body [Korner, 2011; Turner, 2015]. It may be the case that ALS pathology has a number of focal points of origin which act as triggers to the spread of pathology in the brain. In fact, a VBM study by Bede et al. (2013) found that focal degeneration in the motor cortex of ALS patients corresponded with the areas of symptom onset for these individuals. While the motor cortex may be one of these areas, the internal capsule might be another area of major pathology or onset. Given that the internal capsule demonstrated some of the most significant degeneration as measured by texture and this also correlated with clinical UMN signs and BPF, the internal capsule should be investigated as a focal region of differentiation in the diagnostic process. To further bolster this claim, an ROC analysis was done which examined discrimination of ALS patients and healthy controls using texture values from

the internal capsule. This model, once corrected for age and site of acquisition, was statistically significant for each of the features in question. The ROCs consistently reported relatively high sensitivity and specificity (Table 10). These values were rather strong in contrast to patient-control differentiation typically reported from studies of conventional MRI including visual assessment of T1 images [Gupta, 2014; Grosskreutz, 2008; Kalra and Arnold, 2003; Kassubek, 2012]. This helps to solidify TA as an improvement on conventional imaging and suggests that analysis of T1 images has a potential use as a diagnostic measure. While a whole brain voxel-wise analysis may not show significant results for each feature due to a less stark difference between groups, the ROC demonstrates that each texture feature's values can divide the sample into groups based on their diagnosis. Obviously, this comparison is simplified compared to a clinical examination due to strict inclusion and exclusion criteria. In the process of diagnosis, neurologists would have to differentiate between not only ALS and controls, but also any and all disease mimics. However, it does provide a promising outlook for future studies and how the technique might be applied as part of the diagnostic process for ALS. Furthermore, the use of TA in conjunction with other neuroimaging methods may improve sensitivity and specificity in diagnostic measures. More research should be done to investigate this. Future research should seek to include patients earlier on in the disease process. If possible, the most ideal subjects would be people who have not yet been diagnosed. Tracking these patients longitudinally would allow an examination of the disease in comparison to other potential mimics to determine whether the internal capsule is an effective area of interest for differentiation in the diagnostic process.

The CALSNIC protocol was created as a multicentre initiative to develop a framework for standardised imaging and other analysis methods in ALS research. As was previously

mentioned, all aspects of data acquisition in this study were done prospectively to ensure as little variation as possible between sites. The goal is that if standard rules or guidelines for data acquisition in ALS research are established, then data acquired by future studies by other groups might by combined for a collaborative effort. This would be a model similar to the ADNI database, but in this case pertaining to ALS rather than Alzheimer's disease. Larger datasets through collaboration and combination in ALS research would allow for larger scale examinations and subdivisions of patient groups. This is particularly important in a disease like ALS given that the disease itself is so heterogeneous, and large samples are difficult to come by in certain centres due to limitations of recruitment and inclusion/exclusion criteria. Collaboration with standardised data would sidestep this issue leading to a greater ease in the development of new investigative efforts. On a more short-term level, the goals of CALSNIC were to examine different MRI analysis tools and modalities to explore cerebral degeneration in ALS. Data is being acquired longitudinally with neuropsychometrics done at each MRI visit. The collection of data in the CALSNIC was multimodal, but the goal of the present study was to demonstrate the efficacy of TA in the context of an analysis focused on comparisons to clinical measures motor neuron degeneration. However, future studies have the opportunity to explore more multimodal comparisons and tease apart the data with subgroup analyses and post-mortem imaging. As of now there are eight sites included in CALSNIC. This existing collaboration between sites as well as the potential for more sites to follow suit in the future holds promise for development of this framework for the study of ALS and other motor neuron diseases.

One limitation of these results was that they are uncorrected for multiple comparisons. In whole brain, voxel-wise analyses, it is common practice to correct for false positives that can occur when examining such a large number of individual comparisons – one at each voxel.

Correction is typically done by way of False Discovery Rate (FDR) correction, or Family-Wise Error (FWE) correction. When either of these corrections was applied to the results of the present study, they disappear. This introduces a need for caution when interpreting the results, though some of this lack of statistical power may be attributable to the small samples seen at each site and heterogeneity of the patients in those samples. As stated previously, these small samples being made representative of ALS patients at each site can introduce variability in the statistical analysis leading to a decrease in statistical power. The results of the between-sites voxel-wise analysis demonstrate noticeable variability in texture abnormalities detected between sites. However, given that texture was shown to be reliable and reproducible between sites (Experiment 1), these results further enforce sample heterogeneity. Thus, future studies should look to recruit larger samples to mitigate this effect. Nevertheless, given that many of the texture abnormalities detected are present in areas of known ALS pathology, it is reasonable to suggest that these changes are not random. In the process of developing the present study some criteria may have limited its complexity, but these were made with the goal of ensuring effects seen in the results were as much as possible attributed to ALS itself. While the CALSNIC protocol allows the recruitment of motor neuron diseases other than ALS such as PLS and PMA, the present study excluded any patients who were not specifically ALS. This was done to ensure that differences in degeneration for other motor neuron diseases did not skew the results either way. However, this of course means that the differentiation between patients and controls is not necessarily directly representative of a clinical situation. Inclusion was also held back in part by numbers. The total number of other motor neuron disease patients was roughly five participants including all sites. Had there been more, it may have easier to justify inclusion as a subgroup. Future studies should look to analyse these patients as well. Another limitation of the present

study is variation in MRI data between sites of acquisition. As mentioned previously, all data was acquired with a standardised protocol, and all comparisons were corrected for differences between sites. Yet, we still cannot entirely rule out the possibility of some inter-site variability in MRI. This also applies to neurological evaluations including ALSFRS-R and tapping scores. The same metrics administered by different physicians and researchers at each site can contribute to an overall added variability in the data. Regardless of standard protocol to follow, there is some subjectivity in each of these types of analysis which can theoretically be a source of heterogeneity in our overall sample. While these measures are corrected for site differences, this remains a limitation of this study as it would be a consideration in any multicentre analysis. One final limitation of the current study is a limitation of the vast majority of all ALS-related literature. However, this limitation is more so an opportunity for future steps. One of the greatest difficulties in the diagnostic process of ALS is in early recognition and differentiation of the disease from other similar and mimicking disorders, yet typically the patients included in ALS research are those who have already been diagnosed with some certainty. In an ideal scenario, there would be a greater outreach to family doctors and those seeing patients at their first symptom onset. Recruitment and longitudinal analysis of patients prior to diagnosis would be extremely useful in studying the way that ALS develops uniquely in the brain compared to other conditions that might mimic it. Furthermore, it would allow the application of tools such as TA firstly, to determine the differences between those who go on to develop ALS and those who don't, and secondly, to further use these differences to help expediate future diagnoses. Of course, there are sure to be challenges in recruiting patients who have not yet been diagnosed, but this should be a goal for future analyses.

One of the most important triumphs of the present study is the detection of ALS pathology in both GM and WM using only clinical T1-weighted images. This is only bolstered by the fact that the cerebral degeneration in ALS patients which was detected appears to be of variable pathological classification. A challenge that is often seen in the application of MRI as a diagnostic tool is a requirement of a multitude of scan sequences to analyse all bases. For some disorders this is not a necessity. MS lesions can be seen as hyperintense areas on a T2-weighted image, and Alzheimer's pathology can be seen as significant atrophic change throughout the brain on a T1-weighted image [Jack Jr., 2008; Dustin, 2016; Rashid, 2008]. In the case of ALS, we are not so lucky, as there are rarely obvious differences between an ALS patient and a control on a structural image. Instead, GM and WM integrity can be examined separately using VBM and DTI, or neuronal health can be examined by way of MRS. In contrast, the current study's findings indicate that this may no longer be the case. Given that TA can examine the whole brain with only a clinical T1-weighted image, it is a tool that is easily applicable in clinical settings. Not only are T1 scans done during the diagnostic process for most ALS patients, but they are also relatively quick and easy for patients. The speed at which the scan can be completed is particularly important for patients experiencing bulbar dysfunction as they may have difficulty with excessive salivation, swallowing, and clearing their throats. If further research demonstrates that TA is truly an effective tool, translation to clinical application would be relatively simple. Adding a T1-weighted scan to the early diagnostic process would allow for both a whole brain and ROI-based analysis of patients to objectively measure disease presence. If patients are diagnosed earlier, it allows for these patients to start treatment more quickly, hopefully at a point where the pathology can be slowed or even stopped. Even if TA is not proven to be the be-all-end-all tool for diagnosis, it can at least act as a supplement to diagnosis and a tool used to track

progression objectively. This of course allows for a less subjective examination of drug trial efficacy and the trajectory of the disease itself rather than relying on reports from patients and clinical measures which can be difficult to measure with certainty due to other pathology present.

6.5. Conclusion

The results of Experiment 2 have demonstrated that TA is capable of detecting pathological changes in the brain due to ALS. These texture abnormalities were present in the motor regions of the brain as well as other extra-motor regions. Furthermore, texture abnormalities may be attributable to various pathological processes. This should be investigated further in future studies which combine the use of TA and post-mortem tissue analysis with the goal of linking specific texture changes with specific pathologies in the brain. In addition to these results, it was determined that texture values correlated with clinical UMN burden and global brain atrophy as measured by BPF. Texture in the internal capsule was also found to be predictive of diagnosis between patients and controls. While TA needs to be tested further before implementation in clinical settings, it does hold promise as a potential biomarker for ALS patients. Given that TA is capable of examining whole-brain degeneration using T1 structural images, it presents a relatively simple solution to other diagnostic strategies.

7. Bibliography

Abdulla, S. (2017). T1, T2 and PD weighted imaging Retrieved from https://www.radiologycafe.com/radiology-trainees/frcr-physics-notes/t1-t2-and-pd-weighted-imaging

Abe, K., Fujimura, H., Toyooka, K., Hazama, T., Hirono, N., Yorifuji, S., & Yanagihara, T. (1993). Single-photon emission computed tomographic investigation of patients with motor-neuron disease. *Neurology, 43*(8), 1569-1573. 10.1212/WNL.43.8.1569

Abrahams, S., Goldstein, L. H., Simmons, A., Brammer, M., Williams, S. C. R., Giampietro, V., & Leigh, P. N. (2004). Word retrieval in amyotrophic lateral sclerosis: A functional magnetic resonance imaging study. *Brain, 127*, 1507-1517. 10.1093/brain/awh170

Al-Chalabi, A., Jones, A., Troakes, C., King, A., Al-Sarraj, S., & van den Berg, Leonard H. (2012). The genetics and neuropathology of amyotrophic lateral sclerosis. *Acta Neuropathologica, 124*(3), 339-352. 10.1007/s00401-012-1022-4

Alexander, A. L., Lee, J. E., Lazar, M., & Field, A. S. (2007). Diffusion tensor imaging of the brain. *Neurotherapeutics, 4*(3), 316-329. 10.1016/j.nurt.2007.05.011

Al-Sarraj, S., King, A., Troakes, C., Smith, B., Maekawa, S., Bodi, I., . . . Shaw, C. E. (2011). p62 positive, TDP-43 negative, neuronal cytoplasmic and intranuclear inclusions in the cerebellum and hippocampus define the pathology of C9orf72-linked FTLD and MND/ALS. *Acta Neuropathologica, 122*(6), 691-702. 10.1007/s00401-011-0911-2

Antel, S. B., Collins, D. L., Bernasconi, N., Andermann, F., Shinghal, R., Kearney, R. E., . . . Bernasconi, A. (2003). Automated detection of focal cortical dysplasia lesions using computational models of their MRI characteristics and texture analysis. *Neuroimage, 19*(4), 1748-1759. 10.1016/S1053-8119(03)00226-X

Ashburner, J., & Friston, K. (2009). *Statistical parametric mapping, version 8 (SPM8)*

Bastin, M. E., Pettit, L. D., Bak, T. H., Gillingwater, T. H., Smith, C., & Abrahams, S. (2013). Quantitative tractography and tract shape modeling in amyotrophic lateral sclerosis. *Journal of Magnetic Resonance Imaging, 38*(5), 1140-1145. 10.1002/jmri.24073

Bede, P., Bokde, A., Elamin, M., Byrne, S., McLaughlin, R., Fagan, A., & Hardiman, O. (2013). Grey matter correlates of clinical variables in amyotrophic lateral sclerosis - A neuroimaging study of ALS motor phenotype heterogeneity and cortical focality. *Neurology, 80*

Beghi, E., Pupillo, E., Messina, P., Giussani, G., Chio, A., Zoccolella, S., . . . Logroscino, G. (2011). Coffee and amyotrophic lateral sclerosis: A possible preventive role. *Neurology, 76*(9), A113.

Bonilha, L., Kobayashi, E., Castellano, G., Coelho, T., Tinois, E., Cendes, F., & Li, L. M. (2003). Texture analysis of hippocampal sclerosis.*Epilepsia, 44*(12), 1546-1550. 10.1111/j.0013-9580.2003.27103.x

Branco, L. M. T., De Albuquerque, M., De Andrade, Helen Maia T, Bergo, F. P. G., Nucci, A., & Franca, M. C. (2014). Spinal cord atrophy correlates with disease duration and severity in amyotrophic lateral sclerosis. *Amyotrophic Lateral Sclerosis and Frontotemporal Degeneration, 15*(1-2), 93-97. 10.3109/21678421.2013.852589

Brettschneider, J., Del Tredici, K., Toledo, J. B., Robinson, J. L., Irwin, D. J., Grossman, M., . . . Trojanowski, J. Q. (2013). Stages of pTDP-43 pathology in amyotrophic lateral sclerosis. *Annals of Neurology, 74*(1), 20-38. 10.1002/ana.23937

Brettschneider, J., Libon, D. J., Toledo, J. B., Xie, S. X., McCluskey, L., Elman, L., . . . Trojanowski, J. Q. (2012). Microglial activation and TDP-43 pathology correlate with executive dysfunction in amyotrophic lateral sclerosis. *Acta Neuropathologica, 123*(3), 395-407. 10.1007/s00401-011-0932-x

Cardenas-Blanco, A., Machts, J., Acosta-Cabronero, J., Kaufmann, J., Abdulla, S., Kollewe, K., . . . Nestor, P. J. (2016). Structural and diffusion imaging versus clinical assessment to monitor amyotrophic lateral sclerosis. *Neuroimage-Clinical, 11*, 408-414. 10.1016/j.nicl.2016.03.011

Chaddad, A., & Tanougast, C. (2016). Extracted magnetic resonance texture features discriminate between phenotypes and are associated with overall survival in glioblastoma

multiforme patients. *Medical & Biological Engineering & Computing, 54*(11), 1707-1718. 10.1007/s11517-016-1461-5

Chan, S., Shungu, D. C., Douglas-Akinwande, A., Lange, D. J., & Rowland, L. P. (1999). Motor neuron diseases: Comparison of single-voxel proton MR spectroscopy of the motor cortex with MR imaging of the brain. *Radiology, 212*(3), 763-769. 10.1148/radiology.212.3.r99au35763

Chang, J. L., Lomen-Hoerth, C., Murphy, J., Henry, R. G., Kramer, J. H., Miller, B. L., & Gorno-Tempini, M. L. (2005). A voxel-based morphometry study of patterns of brain atrophy in ALS and ALS/FTLD. *Neurology, 65*(1), 75-80. 10.1212/01.wnl.0000167602.38643.29

Chapman, M. C., Jelsone-Swain, L., Johnson, T. D., Gruis, K. L., & Welsh, R. C. (2014). Diffusion tensor MRI of the corpus callosum in amyotrophic lateral sclerosis. *Journal of Magnetic Resonance Imaging, 39*(3), 641-647. 10.1002/jmri.24218

Chiò, A., Pagani, M., Agosta, F., Calvo, A., Cistaro, A., & Filippi, M. (2014). Neuroimaging in amyotrophic lateral sclerosis: Insights into structural and functional changes. *The Lancet Neurology, 13*(12), 1228-1240. 10.1016/S1474-4422(14)70167-X Retrieved from http://www.thelancet.com.login.ezproxy.library.ualberta.ca/journals/laneur/article/PIIS1474-4422(14)70167-X/abstract

Cui, X., Li, J., Song, X., & Ma, Z. (2016). *xjView*

Darling, E., & Joseph, R. (1968). Pattern recognition from satellite altitudes. *Ieee Transactions on Systems Science and Cybernetics, SSC4*(1), &. 10.1109/TSSC.1968.300186

de Albuquerque, M., Anjos, L. G. V., Tavares de Andrade, Helen Maia, de Oliveira, M. S., Castellano, G., Ribeiro de Rezende, Thiago Junqueira, . . . Franca Junior, M. C. (2016). MRI texture analysis reveals deep gray nuclei damage in amyotrophic lateral sclerosis. *Journal of Neuroimaging, 26*(2), 201-206. 10.1111/jon.12262

de Carvalho, M., & Swash, M. (2011). Amyotrophic lateral sclerosis: An update. *Current Opinion in Neurology, 24*(5), 497-503. 10.1097/WCO.0b013e32834916a9

Demler, T. L. (2017). Introduction to pseudobulbar affect: Setting the stage for recognition and familiarity with this challenging disorder.*American Journal of Managed Care, 23*(18), S344.

Devine, M. S., Pannek, K., Coulthard, A., McCombe, P. A., Rose, S. E., & Henderson, R. D. (2015). Exposing asymmetric gray matter vulnerability in amyotrophic lateral sclerosis. *Neuroimage-Clinical, 7*, 782-787. 10.1016/j.nicl.2015.03.006

Doan, N. T., van den Bogaard, Simon J A, Dumas, E. M., Webb, A. G., van Buchem, M. A., Roos, R. A. C., . . . Milles, J. (2014). Texture analysis of ultrahigh field T-2*-weighted MR images of the brain: Application to huntington's disease. *Journal of Magnetic Resonance Imaging, 39*(3), 633-640. 10.1002/jmri.24199

Dustin, D., Hall, B. M., Annapragada, A., & Pautler, R. G. (2016). Neuroimaging in alzheimer's disease: Preclinical challenges toward clinical efficacy. *Translational Research, 175*, 37-53. 10.1016/j.trsl.2016.03.005

Eisen, A., & Weber, M. (2001). The motor cortex and amyotrophic lateral sclerosis. *Muscle & Nerve, 24*(4), 564-573. 10.1002/mus.1042

Fang, F., & Ye, W. (2010). Smoking may be considered an established risk factor for sporadic als. *Neurology, 74*(23), 1927-1927. 10.1212/WNL.0b013e3181e038e9

Focke, N. K., Helms, G., Kaspar, S., Diederich, C., Tóth, V., Dechent, P., . . . Paulus, W. (2011). Multi-site voxel-based morphometry — not quite there yet. *NeuroImage, 56*(3), 1164-1170. 10.1016/j.neuroimage.2011.02.029 Retrieved from http://www.sciencedirect.com.login.ezproxy.library.ualberta.ca/science/article/pii/S1053811911001856

Freedman, D. M., Kuncl, R. W., Weinstein, S. J., Malila, N., Virtamo, J., & Albanes, D. (2013). Vitamin E serum levels and controlled supplementation and risk of amyotrophic lateral sclerosis. *Amyotrophic Lateral Sclerosis and Frontotemporal Degeneration, 14*(4), 246-251. 10.3109/21678421.2012.745570

Furukawa, Y., & O'Halloran, T. V. (2005). Amyotrophic lateral sclerosis mutations have the greatest destabilizing effect on the apo- and reduced form of SOD1, leading to unfolding

and oxidative aggregation. *Journal of Biological Chemistry, 280*(17), 17266-17274. 10.1074/jbc.M500482200

Gordon, P. H., Artaud, F., Aouba, A., Laurent, F., Meininger, V., & Elbaz, A. (2011). Changing mortality for motor neuron disease in france (1968-2007): An age-period-cohort analysis. *European Journal of Epidemiology, 26*(9), 729-737. 10.1007/s10654-011-9595-0

Grosskreutz, J., Peschel, T., Unrath, A., Dengler, R., Ludolph, A. C., & Kassubek, J. (2008). Whole brain-based computerized neuroimaging in ALS and other motor neuron disorders. *Amyotrophic Lateral Sclerosis, 9*(4), 238-248. 10.1080/17482960802163622

Gupta, A., Nguyen, T. B., Chakraborty, S., & Bourque, P. R. (2014). Accuracy of conventional MRI in ALS. *Canadian Journal of Neurological Sciences, 41*(1), 53-57. 10.1017/S0317167100016267

Hammer, R., Tomiyasu, U., & Scheibel, A. (1979). Degeneration of the human betz cell due to amyotrophic lateral sclerosis. *Experimental Neurology, 63*(2), 336-346. 10.1016/0014-4886(79)90129-8

Hecht, M. J., Fellner, F., Fellner, C., Hilz, M. J., Heuss, D., & Neundorfer, B. (2001). MRI-FLAIR images of the head show corticospinal tract alterations in ALS patients more frequently than T2-, T1- and proton-density-weighted images. *Journal of the Neurological Sciences, 186*(1-2), 37-44. 10.1016/S0022-510X(01)00503-2

Helms, G., Draganski, B., Frackowiak, R., Ashburner, J., & Weiskopf, N. (2009). Improved segmentation of deep brain grey matter structures using magnetization transfer (MT) parameter maps. *Neuroimage, 47*(1), 194-198. 10.1016/j.neuroimage.2009.03.053

Introna, A., D'Errico, E., Modugno, B., Scarafino, A., Fraddosio, A., Distaso, E., . . . Simone, I. L. (2018). Adherence to riluzole in patients with amyotrophic lateral sclerosis: An observational study. *Neuropsychiatric Disease and Treatment, 14*, 193-203. 10.2147/NDT.S150550

Iyer, A. K., Jones, K. J., Sanders, V. M., & Walker, C. L. (2018). Temporospatial analysis and new players in the immunology of amyotrophic lateral sclerosis. *International Journal of Molecular Sciences, 19*(2), 631. 10.3390/ijms19020631

Jack, C. R., Bernstein, M. A., Fox, N. C., Thompson, P., Alexander, G., Harvey, D., . . . Weiner, M. W. (2008). The alzheimer's disease neuroimaging initiative (ADNI): MRI methods. *Journal of Magnetic Resonance Imaging, 27*(4), 685-691. 10.1002/jmri.21049

Jackson, E. F., Ginsberg, L. E., Schomer, D. F., & Leeds, N. E. (1997). A review of MRI pulse sequences and techniques in neuroimaging.*Surgical Neurology, 47*(2), 185-199. 10.1016/S0090-3019(96)00375-8

Jaiswal, M. K., Zech, W., Goos, M., Leutbecher, C., Ferri, A., Zippelius, A., . . . Keller, B. U. (2009). Impairment of mitochondrial calcium handling in a mtSOD1 cell culture model of motoneuron disease. *Bmc Neuroscience, 10*, 64. 10.1186/1471-2202-10-64

Kalra, S., & Arnold, D. (2003). Neuroimaging in amyotrophic lateral sclerosis. *Amyotrophic Lateral Sclerosis and Other Motor Neuron Disorders, 4*(4), 243-248. 10.1080/14660820310011269

Kamel, F., Umbach, D. M., Bedlack, R. S., Richards, M., Watson, M., Alavanja, M. C. R., . . . Sandler, D. P. (2012). Pesticide exposure and amyotrophic lateral sclerosis. *Neurotoxicology, 33*(3), 457-462. 10.1016/j.neuro.2012.04.001

Kassner, A., & Thornhill, R. E. (2010). Texture Analysis: A Review of Neurologic MR Imaging Applications. *American Journal of Neuroradiology, 31*(5), 809-816. 10.3174/ajnr.A2061

Kassubek, J., Ludolph, A. C., & Mueller, H. (2012). Neuroimaging of motor neuron diseases. *Therapeutic Advances in Neurological Disorders, 5*(2), 119-127. 10.1177/1756285612437562

Keller, J., Vymazal, J., Ridzon, P., Rusina, R., Kulist'ak, P., Malikova, H., . . . Jech, R. (2011). Quantitative brain MR imaging in amyotrophic lateral sclerosis. *Magnetic Resonance Materials in Physics Biology and Medicine, 24*(2), 67-76. 10.1007/s10334-010-0237-4

Kim, H. -., Oh, S. -., de Leon, M., Wang, X., Oh, K. -., Park, J. -., . . . Kim, S. H. (2017). Structural explanation of poor prognosis of amyotrophic lateral sclerosis in the non-demented state. *European Journal of Neurology, 24*(1), 122-129. 10.1111/ene.13163

Kim, H., de Leon, M., Wang, X., Kim, H. Y., Lee, Y., Kim, Y., & Kim, S. H. (2017). Relationship between clinical parameters and brain structure in sporadic amyotrophic lateral sclerosis patients according to onset type: A voxel-based morphometric study. *Plos One, 12*(1), e0168424. 10.1371/journal.pone.0168424

Koerner, S., Kollewe, K., Fahlbusch, M., Zapf, A., Dengler, R., Krampfl, K., & Petri, S. (2011). Onset and spreading patterns of upper and lower motor neuron symptoms in amyotrophic lateral sclerosis. *Muscle & Nerve, 43*(5), 636-642. 10.1002/mus.21936

Komander, D. (2009). The emerging complexity of protein ubiquitination. *Biochemical Society Transactions, 37*, 937-953. 10.1042/BST0370937

Kraemer, B. C., Schuck, T., Wheeler, J. M., Robinson, L. C., Trojanowski, J. Q., Lee, V. M. Y., & Schellenberg, G. D. (2010). Loss of murine TDP-43 disrupts motor function and plays an essential role in embryogenesis. *Acta Neuropathologica, 119*(4), 409-419. 10.1007/s00401-010-0659-0

Kruggel, F., Turner, J., & Muftuler, L. T. (2010). Impact of scanner hardware and imaging protocol on image quality and compartment volume precision in the ADNI cohort. *Neuroimage, 49*(3), 2123-2133. 10.1016/j.neuroimage.2009.11.006

Kumar, V., Islam, A., Hassan, M. I., & Ahmad, F. (2016). Therapeutic progress in amyotrophic lateral sclerosis-beginning to learning. *European Journal of Medicinal Chemistry, 121*, 903-917. 10.1016/j.ejmech.2016.06.017

Lancaster, J., & Martinez, M. (2006). *Mango (multi-image analysis GUI)*. University of Texas Health Science Centre, Research Imaging Institute:

Langefeld, C. D. (2013). Age of onset of amyotrophic lateral sclerosis is modulated by a locus on 1p34.1. *Neurobiology of Aging, 34*(1), 357.e7. 10.1016/j.neurobiolaging.2012.07.017

Lerski, R. A., Schad, L. R., Luypaert, R., Amorison, A., Muller, R. N., Mascaro, L., . . . Bruno, A. (1999). Multicentre magnetic resonance texture analysis trial using reticulated foam test objects. *Magnetic Resonance Imaging, 17*(7), 1025-1031. 10.1016/S0730-725X(99)00034-X

Lillo, P., Mioshi, E., Burrell, J. R., Kiernan, M. C., Hodges, J. R., & Hornberger, M. (2012). Grey and white matter changes across the amyotrophic lateral sclerosis-frontotemporal dementia continuum. *Plos One, 7*(8), e43993. 10.1371/journal.pone.0043993

Lule, D., Diekmann, V., Anders, S., Kassubek, J., Kuebler, A., Ludolph, A. C., & Birbaumer, N. (2007). Brain responses to emotional stimuli in patients with amyotrophic lateral sclerosis (ALS). *Journal of Neurology, 254*(4), 519-527. 10.1007/s00415-006-0409-3

Maani, R., Yang, Y. H., & Kalra, S. (2015). Voxel-based texture analysis of the brain. *Plos One, 10*(3), e0117759. 10.1371/journal.pone.0117759

Maani, R., Yang, Y., Emery, D., & Kalra, S. (2016). Cerebral degeneration in amyotrophic lateral sclerosis revealed by 3-dimensional texture analysis. *Frontiers in Neuroscience, 10*, 120. 10.3389/fnins.2016.00120

Mackenzie, I. R. A., Rademakers, R., & Neumann, M. (2010). TDP-43 and FUS in amyotrophic lateral sclerosis and frontotemporal dementia.*Lancet Neurology, 9*(10), 995-1007. 10.1016/S1474-4422(10)70195-2

Maggi, P., Absinta, M., Grammatico, M., Vuolo, L., Emmi, G., Carlucci, G., . . . Massacesi, L. (2018). Central vein sign differentiates multiple sclerosis from central nervous system inflammatory vasculopathies. *Annals of Neurology, 83*(2), 283-294. 10.1002/ana.25146

Manev, H., Costa, E., Wroblewski, J., & Guidotti, A. (1990). Abusive stimulation of excitatory amino-acid receptors - a strategy to limit neurotoxicity. *Faseb Journal, 4*(10), 2789-2797.

Martin, D., Thompson, M. A., Nadler, J. V. (1993). The neuroprotective agent riluzole inhibits release of L-glutamate and L-aspartate from slices of hippocampal area CA1. *European Journal of Pharmacology, 250*(3), 473-476. 10.1016/0014-2999(93)90037-I

Masuda, M., Senda, J., Watanabe, H., Epifanio, B., Tanaka, Y., Imai, K., . . . Sobue, G. (2016). Involvement of the caudate nucleus head and its networks in sporadic amyotrophic lateral sclerosis-frontotemporal dementia continuum. *Amyotrophic Lateral Sclerosis and Frontotemporal Degeneration, 17*(7-8), 571-579. 10.1080/21678421.2016.1211151

Maurel, C., Dangoumau, A., Marouillat, S., Bulard, C., Chami, A., Hergesheimer, R., . . . Vourc'h, P. (2018). Causative Genes in Amyotrophic Lateral Sclerosis and Protein Degradation Pathways: a Link to Neurodegeneration. *Molecular Neurobiology, 2018 Jan 10.* 10.1007/s12035-017-0856-0

Mayerhoefer, M. E., Szomolanyi, P., Jirak, D., Materka, A., & Trattnig, S. (2009). Effects of MRI acquisition parameter variations and protocol heterogeneity on the results of texture analysis and pattern discrimination: An application-oriented study. *Medical Physics, 36*(4), 1236-1243. 10.1118/1.3081408

Menke, R. a. L., Proudfoot, M., Talbot, K., & Turner, M. R. (2018). The two-year progression of structural and functional cerebral MRI in amyotrophic lateral sclerosis. *Neuroimage-Clinical, 17*, 953-961. 10.1016/j.nicl.2017.12.025

Mittal, S., Wu, Z., Neelavalli, J., & Haacke, E. M. (2009). Susceptibility-weighted imaging: Technical aspects and clinical applications, part 2.*American Journal of Neuroradiology, 30*(2), 232-252. 10.3174/ajnr.A1461

Mueller, H., Turner, M. R., Grosskreutz, J., Abrahams, S., Bede, P., Govind, V., . . . Kassubek, J. (2016). A large-scale multicentre cerebral diffusion tensor imaging study in amyotrophic lateral sclerosis. *Journal of Neurology Neurosurgery and Psychiatry, 87*(6), 570-579. 10.1136/jnnp-2015-311952

Natarajan, C., & Takeda, K. (2017). Regulation of various DNA repair pathways by E3 ubiquitin ligases. *Journal of Cancer Research and Therapeutics, 13*(2), 157-169. 10.4103/0973-1482.204879

Okamoto, K., Kihira, T., Kondo, T., Kobashi, G., Washio, M., Sasaki, S., . . . Nagai, M. (2009). Lifestyle factors and risk of amyotrophic lateral sclerosis: A case-control study in japan. *Annals of Epidemiology, 19*(6), 359-364. 10.1016/j.annepidem.2009.01.015

Oppedal, K., Eftestol, T., Engan, K., Beyer, M. K., & Aarsland, D. (2015). Classifying dementia using local binary patterns from different regions in magnetic resonance images. *International Journal of Biomedical Imaging,* , 572567. 10.1155/2015/572567

Pereira, J. M. S., Xiong, L., Acosta-Cabronero, J., Pengas, G., Williams, G. B., & Nestor, P. J. (2010). Registration accuracy for VBM studies varies according to region and degenerative disease grouping. *Neuroimage, 49*(3), 2205-2215. 10.1016/j.neuroimage.2009.10.068

Preston, D. C. (2006). Magnetic resonance imaging (MRI) of the brain and spine: Basics Retrieved from http://casemed.case.edu/clerkships/neurology/Web%20Neurorad/MRI%20Basics.htm

Prudlo, J., Bissbort, C., Glass, A., Grossmann, A., Hauenstein, K., Benecke, R., & Teipel, S. J. (2012). White matter pathology in ALS and lower motor neuron ALS variants: A diffusion tensor imaging study using tract-based spatial statistics. *Journal of Neurology, 259*(9), 1848-1859. 10.1007/s00415-012-6420-y

Rajagopalan, V., & Pioro, E. P. (2014). Distinct patterns of cortical atrophy in ALS patients with or without dementia: An MRI VBM study.*Amyotrophic Lateral Sclerosis and Frontotemporal Degeneration, 15*(3-4), 216-225. 10.3109/21678421.2014.880179

Rajagopalan, V., & Pioro, E. P. (2015). Disparate voxel based morphometry (VBM) results between SPM and FSL softwares in ALS patients with frontotemporal dementia: Which VBM results to consider? *Bmc Neurology, 15*, 32. 10.1186/s12883-015-0274-8

Rascovsky, K., Hodges, J. R., Knopman, D., Mendez, M. F., Kramer, J. H., Neuhaus, J., . . . Miller, B. L. (2011). Sensitivity of revised diagnostic criteria for the behavioural variant of frontotemporal dementia. *Brain, 134*, 2456-2477. 10.1093/brain/awr179

Rashid, W., & Miller, D. H. (2008). Recent advances in neuroimaging of multiple sclerosis. *Seminars in Neurology, 28*(1), 46-55. 10.1055/s-2007-1019127

Roberts, A. L., Johnson, N. J., Chen, J. T., Cudkowicz, M. E., & Weisskopf, M. G. (2016). Race/ethnicity, socioeconomic status, and ALS mortality in the united states. *Neurology, 87*(22), 2300-2308. 10.1212/WNL.0000000000003298

Rooney, W. D., Miller, R. G., Gelinas, D., Schuff, N., Maudsley, A. A., & Weiner, M. W. (1998). Decreased N-acetylaspartate in motor cortex and corticospinal tract in ALS. *Neurology, 50*(6), 1800-1805. 10.1212/WNL.50.6.1800

Saberi, S., Stauffer, J. E., Schulte, D. J., & Ravits, J. (2015). Neuropathology of amyotrophic lateral sclerosis and its variants. *Neurologic Clinics, 33*(4), +. 10.1016/j.ncl.2015.07.012

Sankar, T., Bernasconi, N., Kim, H., & Bernasconi, A. (2008). Temporal lobe epilepsy: Differential pattern of damage in temporopolar cortex and white matter. *Human Brain Mapping, 29*(8), 931-944. 10.1002/hbm.20437

Sarica, A., Cerasa, A., Valentino, P., Yeatman, J., Trotta, M., Barone, S., . . . Quattrone, A. (2017). The corticospinal tract profile in amyotrophic lateral sclerosis. *Human Brain Mapping, 38*(2), 727-739. 10.1002/hbm.23412

Schuster, C., Elamin, M., Hardiman, O., & Bede, P. (2016). The segmental diffusivity profile of amyotrophic lateral sclerosis associated white matter degeneration. *European Journal of Neurology, 23*(8), 1361-1371. 10.1111/ene.13038

Sea, K., Sohn, S. H., Durazo, A., Sheng, Y., Shaw, B. F., Cao, X., . . . Valentine, J. S. (2015). Insights into the role of the unusual disulfide bond in copper-zinc superoxide dismutase. *Journal of Biological Chemistry, 290*(4), 2405-2418. 10.1074/jbc.M114.588798

Seals, R. M., Hansen, J., Gredal, O., & Weisskopf, M. G. (2016). Physical trauma and amyotrophic lateral sclerosis: A population-based study using danish national registries. *American Journal of Epidemiology, 183*(4), 294-301. 10.1093/aje/kwv169

Shapiro, L.G., Stockman, G.C. (2000). Computer Vision, March 2000. *Pearson, Chapter 7* – Texture Analysis, 235-247. http://nana.lecturer.pens.ac.id/index_files/referensi/computer_vision/Computer%20Vision.pdf

Shepheard, S. R., Chataway, T., Schultz, D. W., Rush, R. A., & Rogers, M. (2014). The extracellular domain of neurotrophin receptor p75 as a candidate biomarker for amyotrophic lateral sclerosis. *Plos One, 9*(1), e87398. 10.1371/journal.pone.0087398

Sikio, M., Holli-Helenius, K. K., Harrison, L. C. V., Ryymin, P., Ruottinen, H., Saunamaki, T., . . . Dastidar, P. (2015). MR image texture in parkinson's disease: A longitudinal study. *Acta Radiologica, 56*(1), 97-104. 10.1177/0284185113519775

Sivak, S., Bittsansky, M., Kurca, E., Turcanova-Koprusakova, M., Grofik, M., Nosal, V., . . . Dobrota, D. (2010). Proton magnetic resonance spectroscopy in patients with early stages of amyotrophic lateral sclerosis. *Neuroradiology, 52*(12), 1079-1085. 10.1007/s00234-010-0685-6

Sorensen, L., Igel, C., Hansen, N. L., Osler, M., Lauritzen, M., Rostrup, E., & Nielsen, M. (2016). Early detection of alzheimer's disease using MRI hippocampal texture. *Human Brain Mapping, 37*(3), 1148-1161. 10.1002/hbm.23091

Stephens, B., Guiloff, R. J., Navarrete, R., Newman, P., Nikhar, N., & Lewis, P. (2006). Widespread loss of neuronal populations in the spinal ventral horn in sporadic motor neuron disease. A morphometric study. *Journal of the Neurological Sciences, 244*(1-2), 41-58. 10.1016/j.jns.2005.12.003

Strong, M. J., Yang, W., Strong, W. L., Leystra-Lantz, C., Jaffe, H., & Pant, H. C. (2006). Tau protein hyperphosphorylation in sporadic ALS with cognitive impairment. *Neurology, 66*(11), 1770-1771. 10.1212/01.wnl.0000218161.15834.db

Strong, M. J., Grace, G. M., Freedman, M., Lomen-Hoerth, C., Woolley, S., Goldstein, L. H., . . . Figlewicz, D. (2009). Consensus criteria for the diagnosis of frontotemporal cognitive and behavioural syndromes in amyotrophic lateral sclerosis. *Amyotrophic Lateral Sclerosis, 10*(3), 131-146. 10.1080/17482960802654364

Sugiyama, M., Takao, M., Hatsuta, H., Funabe, S., Ito, S., Obi, T., . . . Murayama, S. (2013). Increased number of astrocytes and macrophages/microglial cells in the corpus callosum in amyotrophic lateral sclerosis. *Neuropathology, 33*(6), 591-599. 10.1111/neup.12027

Swinnen, B., & Robberecht, W. (2014). The phenotypic variability of amyotrophic lateral sclerosis. *Nature Reviews Neurology, 10*(11), 661-670. 10.1038/nrneurol.2014.184

Takeda, T., Uchihara, T., Mochizuki, Y., Mizutani, T., & Iwata, M. (2007). Memory deficits in amyotrophic and degeneration lateral sclerosis patients with dementia of the perforant pathway - A clinicopathological study. *Journal of the Neurological Sciences, 260*(1-2), 225-230. 10.1016/j.jns.2007.05.010

Tan, R. H., Yang, Y., Kim, W. S., Dobson-Stone, C., Kwok, J. B., Kiernan, M. C., & Halliday, G. M. (2017). Distinct TDP-43 inclusion morphologies in frontotemporal lobar degeneration with and without amyotrophic lateral sclerosis. *Acta Neuropathologica Communications, 5*, 76. 10.1186/s40478-017-0480-2

Tanaka, M., Kondo, S., Hirai, S., Sun, X., Yamagishi, T., & Okamoto, K. (1993). Cerebral blood-flow and oxygen-metabolism in progressive dementia associated with amyotrophic-lateral-sclerosis. *Journal of the Neurological Sciences, 120*(1), 22-28. 10.1016/0022-510X(93)90019-U

Tandan, R., & Bradley, W. G. (1985). Amyotrophic lateral sclerosis: Part 1. clinical features, pathology, and ethical issues in management.*Annals of Neurology, 18*(3), 271-280. Retrieved from https://onlinelibrary-wiley-com.login.ezproxy.library.ualberta.ca/doi/abs/10.1002/abstract

Turner, M. R., Barnwell, J., Al-Chalabi, A., & Eisen, A. (2012). Young-onset amyotrophic lateral sclerosis: Historical and other observations.*Brain, 135*, 2883-2891. 10.1093/brain/aws144

Turner, M. R., Kiernan, M. C., Leigh, P. N., & Talbot, K. (2009). Biomarkers in amyotrophic lateral sclerosis. *Lancet Neurology, 8*(1), 94-109. 10.1016/S1474-4422(08)70293-X

Turner, M. R., & Swash, M. (2015). The expanding syndrome of amyotrophic lateral sclerosis: A clinical and molecular odyssey. *Journal of Neurology, Neurosurgery, and Psychiatry, 86*(6), 667. 10.1136/jnnp-2014-308946 Retrieved from http://www.ncbi.nlm.nih.gov/pubmed/25644224

Turner, M. R., & Verstraete, E. (2015). What does imaging reveal about the pathology of amyotrophic lateral sclerosis? *Current Neurology and Neuroscience Reports, 15*(7), 45. 10.1007/s11910-015-0569-6

van Es, M. A., Hardiman, O., Chio, A., Al-Chalabi, A., Pasterkamp, R. J., Veldink, J. H., & van den Berg, Leonard H. (2017). *Amyotrophic lateral sclerosis*//doi-org.login.ezproxy.library.ualberta.ca/10.1016/S0140-6736(17)31287-4 Retrieved

from http://www.sciencedirect.com.login.ezproxy.library.ualberta.ca/science/article/pii/S0140673617312874

Vance, C., Rogelj, B., Hortobagyi, T., De Vos, K. J., Nishimura, A. L., Sreedharan, J., . . . Shaw, C. E. (2009). Mutations in FUS, an RNA processing protein, cause familial amyotrophic lateral sclerosis type 6. *Science, 323*(5918), 1208-1211. 10.1126/science.1165942

Vu, L. T., & Bowser, R. (2017). Fluid-based biomarkers for amyotrophic lateral sclerosis. *Neurotherapeutics, 14*(1), 119-134. 10.1007/s13311-016-0503-x

Wang, M., Little, J., Gomes, J., Cashman, N. R., & Krewski, D. (2017). Identification of risk factors associated with onset and progression of amyotrophic lateral sclerosis using systematic review and meta-analysis. *Neurotoxicology, 61*, 101-130. 10.1016/j.neuro.2016.06.015

Waragai, M. (1997). MRI and clinical features in amyotrophic lateral sclerosis. *Neuroradiology, 39*(12), 847-851. 10.1007/s002340050518

Waugh, S. A., Lerski, R. A., Bidaut, L., & Thompson, A. M. (2011). The influence of field strength and different clinical breast MRI protocols on the outcome of texture analysis using foam phantoms. *Medical Physics, 38*(9), 5058-5066. 10.1118/1.3622605

Wonderlick, J. S., Ziegler, D. A., Hosseini-Varnamkhasti, P., Locascio, J. J., Bakkour, A., Van der Kouwe, A., . . . Dickerson, B. C. (2009). Reliability of MRI-derived cortical and subcortical morphometric measures: Effects of pulse sequence, voxel geometry, and parallel imaging. *Neuroimage, 44*(4), 1324-1333. 10.1016/j.neuroimage.2008.10.037

Yang, X., Tridandapani, S., Beitler, J.J., Yu, D.S., Yoshida, E.J., Curran, W.J., Liu, T. (2012). Ultrasound GLCM texture analysis of radiation-induced parotid-gland injury in head-and-neck cancer radiotherapy: An in vivo study of late toxicity. *Medical Physics, 39*(9), 5732-5739. 10.1118/1.4747526

Yu, J., Qi, F., Wang, N., Gao, P., Dai, S., Lu, Y., . . . Che, F. (2014). Increased iron level in motor cortex of amyotrophic lateral sclerosis patients: An in vivo MR study. *Amyotrophic Lateral Sclerosis and Frontotemporal Degeneration, 15*(5-6), 357-361. 10.3109/21678421.2014.906618

Yu, O., Mauss, Y., Zollner, G., Namer, I. J., & Chambron, J. (1999). Distinct patterns of active and non-active plaques using texture analysis on brain nmr images in multiple sclerosis patients: Preliminary results. *Magnetic Resonance Imaging, 17*(9), 1261-1267. 10.1016/S0730-725X(99)00062-4